Section 3

MOLECULAR & NANOTECHNOLOGY

Charge-trapping in 1-nm Si Nanoparticles Embedded in a MOS Gate Stack

O.M. Nayfeh, D.A. Antoniadis, K. Mantey, M.H. Nayfeh
Sponsorship: Singapore-MIT Alliance, NSF

The MOS capacitors incorporating *ex-situ* produced, colloidal, highly mono-dispersed, spherical, 1-nm Si nanoparticles were fabricated and evaluated for potential use as charge storage elements in future non-volatile memory devices. The C-V characteristics are well behaved and agree with similarly fabricated zero-nanoparticle control samples and with an ideal simulation. Unlike larger particle systems, the demonstrated memory effect exhibits effectively pure hole storage. The nature of charging (i.e., hole-type vs. electron-type) may be understood in terms of the novel characteristics of ultra-small Si particles: large energy gap, large charging energy, and consequently a small electron affinity [1].

The left shift of the programmed C-V with respect to the uncharged curve of the active device in Figure 1 indicates charging of the particles with holes. With the application of an erase bias, the stored holes are removed. The effectively pure hole-charging characteristic may be understood in terms of properties of the 1-nm particles and their high degree of mono-dispersity. For instance, Quantum Monte Carlo (QMC) and time-dependent local density theory (TDLDT) calculations predict that the energy-gap and the charging energy for Si particles in the 1-3 nm regime rise due to the effects of quantum confinement, and consequently the electron affinity decreases, approaching that of the SiO_2 matrix [2-3]. The excitation and emission measurements of [4] for the 1-nm $Si_{29}H_{24}$ particles used in this study yielded 3.5 eV for the energy gap, the difference between the highest unoccupied molecular orbital (HOMO), and the lowest unoccupied molecular orbital (LUMO). In addition, [5] measured ~ 1.8 eV for the charging energy of individual 1-nm silicon particles by UHV-STM tunneling spectroscopy. Because of the increased band-gap and large charging energy, the electron affinity of 1-nm Si nanoparticles is greatly reduced from that of bulk Si and becomes comparable to that of SiO_2 ~ 1.0 eV. Consequently, there is no or very little conduction band-offset between the nanoparticles and SiO_2, thus inhibiting electron storage in the conduction band of the particle. However, the well-known asymmetry in the electron and hole barrier heights for the Si/SiO2 system (~ 3.1 eV for electrons, and ~ 4.7 eV for holes) maintains a valence band-offset on the order of 1.7 eV between the nanoparticles and SiO_2, suitable for hole-storage in the valence band of the particles. Figure 2 shows a proposed energy band diagram.

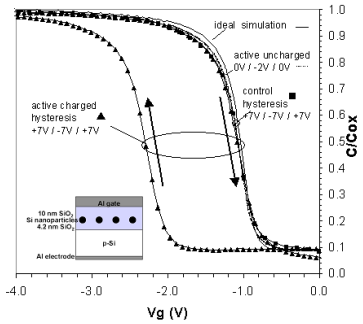

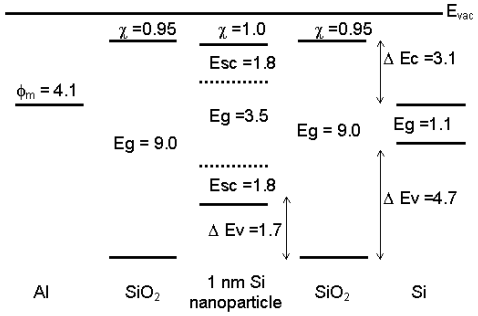

▲ Figure 1: The C-V hysteresis loops. Control and active devices have negligible hysteresis under uncharged conditions (sweeping forward and backward between Vg = 0 V, and Vg = -2.0 V (light-solid, and labeled). Under charging/discharging conditions (sweeping voltage between Vg=+/- 7.0 V, forward and backward), the control device (squares, labeled) has a hysteresis of only ~0.01 V; however, the active device (triangles, labeled) has a hysteresis of ~1.2 V.

▲ Figure 2: Proposed energy band diagram of an MOS system. Shown are adjustments to the band-gap of the 1-nm particles (~ 3.5 eV) and the charging energy (~1.8 eV). There still remains a valence band offset on the order of 1.7 eV for the storage of holes due to the asymmetry in barrier heights for electrons and holes in the Si/SiO2 system.

REFERENCES

[1] O.M. Nayfeh, D.A. Antoniadis, K. Mantey, and M.H. Nayfeh, "Memory effects in metal-oxide-semiconductor capacitors incorporating dispensed highly monodisperse 1 nm silicon nanoparticles," *Applied Physics Letters*, vol. 90, pp. 153105:1-3, Apr. 2007.

[2] S. Rao, J. Sutin, R. Clegg, E. Gratton, M.H. Nayfeh, S. Habbal, A. Tsolakidis and R.M. Martin, "Excited states of tetrahedral single-core Si_{29} nanoparticles," *Physical Review B*, vol. 69, pp. 205319:1-7, May 2004.

[3] D.V. Melnikov and J.R. Chelikowsky, "Electron affinities and ionization energies in Si and Ge nanocrystals," *Physical Review B*, vol. 69, pp. 113305:1-4, Mar. 2004.

[4] G. Belomoin, J. Therrien, A. Smith, S. Rao, S. Chaieb, and M.H. Nayfeh, "Observation of a magic discrete family of ultrabright Si nanoparticles," *Applied Physics Letters*, vol. 80, pp. 841-843, Feb. 2002.

[5] J. Therrien, "Size-dependence of the electrical characteristics of silicon nanoparticles," Ph.D. thesis, University of Illinois at Urbana-Champaign, 2002.

Surface Plasmon Polariton Mediated Energy Transfer in Organic Photovoltaic Devices

T.D. Heidel, J.K. Mapel, K. Celebi, M. Singh, M.A. Baldo
Sponsorship: DARPA/AFOSR, NSF NIRT

With a theoretical efficiency similar to conventional inorganic photovoltaics (PVs) [1] and the potential to be manufactured inexpensively, organic semiconductor technology offers a promising route to ubiquitous solar energy generation. Organic PVs, however, are constrained by a tradeoff between exciton diffusion and optical absorption. The short exciton diffusion length within organic semiconductors demands the use of extremely absorptive materials[2]. Unfortunately, the excitonic character of most organic materials yields highly structured absorption spectra, with regions of strong and weak absorption. We propose a device architecture that boosts the performance of a phthalocyanine-based PV in the absorption gap between the phthalocyanine Q and Soret bands. Light absorption is decoupled from exciton diffusion using a light-absorbing antenna layer external to the conventional charge generating layers (Figure 1). Radiation absorbed by the antenna is transferred into the charge generating layers via surface plasmon polaritons (SPP) in an interfacial thin silver contact. Off resonance, the antenna cavity operates as a reflector and all devices exhibit identical performance. However, in the region where the cavity is tuned to absorb light strongly, the devices with antennas have exhibited increased quantum efficiency of up to 200% compared to those with non-functioning antennas. Peak increases in external quantum efficiency of approximately 80% have been measured for devices with external light absorbing antennas compared to those without.

Energy coupling from external antenna layers into thin film organic PV provides a flexible route to higher efficiency devices. While the introduction of the antenna necessarily adds a step into the energy transduction process, it can be successfully employed in spectral regions where the absorption fraction of the PV cell drops below the SPP-mediated energy transfer efficiency. We measured this latter efficiency to be at least (51±10)%. It is possible to increase the quantum efficiency of an antenna to nearly 100% by optimizing the orientation and position of a luminescent dye with respect to a thin Ag film. Targeting resonant antennas to regions of poor absorption promises to solve a characteristic deficiency of organic PVs.

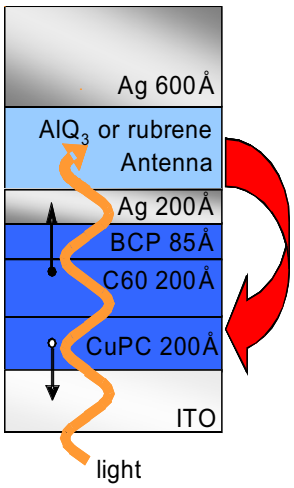

▲ Figure 1: Structure of organic photovoltaic devices with external resonant antenna cavities. We fabricate identical charge generation structures with antennas of varying PL efficiency consisting of isotropic mixtures of AlQ_3 and either 1% of the quenching material CuPC or 1% of the laser dye DCM. Comparing the performance of these devices allows us to isolate the photocurrent originating from light absorbed in the antenna while avoiding interference effects due to changing device structures.

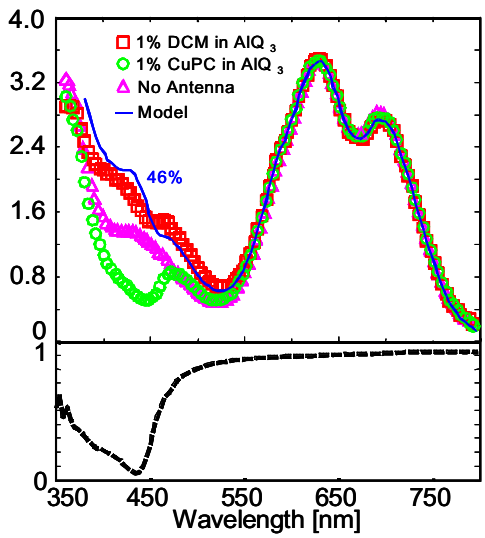

▲ Figure 2: External quantum efficiency (EQE) for resonant antenna devices with functional external AlQ_3-based antenna layers exhibits an increase in EQE over the wavelength range where AlQ_3 absorption occurs and cavity reflectivity decreases. The functional antenna (□) shows a significant performance enhancement versus both the quenched antenna (□) and devices fabricated without any antenna (△). Comparison with modeling (—) indicates that the energy transfer efficiency is approximately 46%.

REFERENCES

[1] S.R. Forrest, "The limits to organic photovoltaic cell efficiency," *MRS Bulletin,* vol. 30, no.1, pp. 28-32, Jan. 2005.

[2] P. Peumans, A. Yakimov, and S.R. Forrest, "Small molecular weight organic thin-film photodetectors and solar cells," *Journal of Applied Physics,* vol. 93, no. 7, pp. 3693-3723, Apr. 2003.

Reduction of Self-absorption in Luminescent Solar Concentrators (LSC) Using Energy Transfer in Guest/Host Thin Films

M.J. Currie, J.K. Mapel, M.A. Baldo
Sponsorship: DARPA/AFOSR, NSF NIRT

Rapidly rising global demand for silicon solar cells has exceeded the capacity of silicon suppliers, leading to escalating costs and material shortages. The development of high performance solar concentrators could dramatically reduce costs and are, we believe, the most promising solution to this problem. By concentrating the sun's light, energy conversion systems can be deployed that use just a fraction of the silicon required by typical solar cells. In particular, luminescent solar concentrators (LSCs) are an especially economical choice since they have the added benefit of having a large acceptance angle for sunlight, reducing the need for expensive tracking equipment. We show recent advances in the field of organic light emitting devices (OLEDs) can be applied to LSCs.

The operation of an LSC is as follows: (1) Light is absorbed by luminescent chromophores embedded within a waveguide. (2) The chromophores re-emit a photon of lower energy, and some portion of the emitted light is confined in the waveguide by total internal reflection. (3) The trapped light is guided to a photovoltaic cell.

Laser dyes are typical choices for LSC chromophores [1], and core-shell quantum dots have also been investigated [2]. Typically a combination of dyes or quantum dots is required to cover the entire solar spectrum, but both dyes and quantum dot suffer from a low quantum yield for emission in the infrared. The other significant limitation in a LSC is re-absorption of trapped light by neighboring chromophores in the waveguide.

OLED fabrication techniques allow us to precisely control the physical distance between chromophores [3], and we are able to achieve resonant energy transfer to a terminal chromophore optimized for quantum yield and self-absorption. This process is repeated with each additional chromophore with the goal of complete coverage of the solar spectrum from the visible to the near infrared.

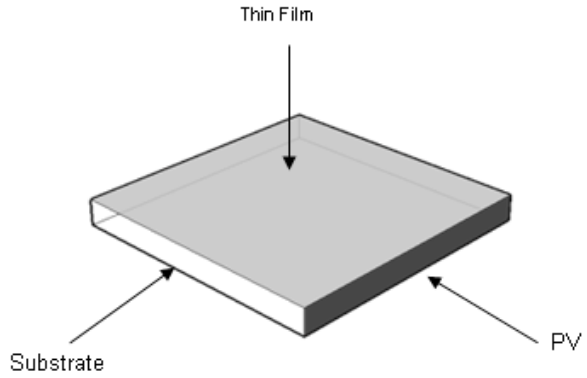

▲ Figure 1: Schematic of a luminescent solar concentrator (LSC). Thin film absorber is applied over a transparent substrate. Photovoltaic is mounted to an edge.

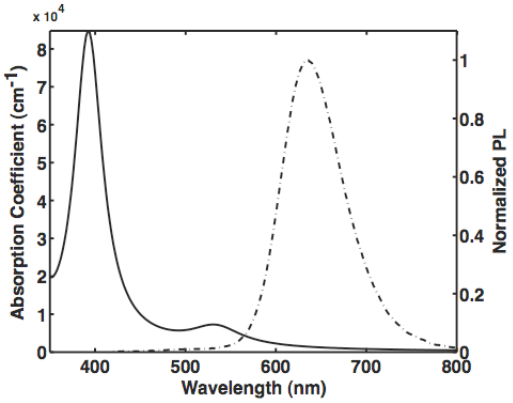

▲ Figure 2: Absorption and photoluminescence spectra of a two-dye LSC.

REFERENCES

[1] A.J. Chatten, K.W.J. Barnham, B.F. Buxton, N.J. Ekins-Daukes and M.A. Malik, "Quantum dot solar concentrators," *Semiconductors*, vol. 38, pp. 909-917, 2004.

[2] S.T. Bailey, G.E. Lokey, M.S. Hanes, J.D.M. Shearer, J.B. McLafferty, G.T. Beaumont, T.T. Baseler , J.M. Layhue, D.R. Broussard, Y.Z. Zhang, and B.P. Wittmershaus. "Optimized excitation energy transfer in a three-dye luminescent solar concentrator," *Solar Energy Materials and Solar Cells*, vol. 91, no. 1, pp. 67-75, 2007.

[3] G.Y. Zhong, J. He, S.T. Zhang, Z. Xu, Z.H. Xiong, H.Z. Shi, X.M. Ding, W. Huang, X.Y. Hou, "*In situ* photoluminescence investigation of doped Alq," *Applied Physics Letters*, vol. 80, no. 25, pp. 4846-4848, 2002.

Kelvin Probe Microscopy of Organic Electronic Devices

K. Milaninia, K. Celebi, M.A. Baldo
Sponsorship: DuPont-MIT Alliance

Kelvin Probe Microscopy (KPM) [1] may be used to determine the contact potential difference between different materials using scanning force microscopy. It has been employed previously in the study of organic semiconductor surfaces and interfaces [2]. We are applying KPM to the channel of an organic field effect transistor to determine the density of states [3]. The technique measures changes in the surface potential of the channel in response to changes in the gate potential relative to a grounded source and drain electrode. The measurement setup is shown in Figure 1. In an ordered semiconductor with energy bands and no states in the gap, the surface potential is expected to vary linearly with the gate before being pinned at threshold by the large density of states at the band edge. But in a disordered semiconductor with an energetic dispersion of localized states, the transition at the threshold voltage is expected to be blurred. Figure 2a shows the initial results for the hole transporting organic semiconductor copper phthalocyanine (CuPC). The CuPC is observed to have a broad density of states that stretch well into the gap between its highest occupied molecular orbital (HOMO) and its lowest unoccupied molecular orbital (LUMO). In Figure 2b we plot the density of states as calculated from the relation

$$DOS = C_G / q^2 (dV_{GS}/dU - 1)$$

where DOS is the density of states per unit energy, C_G is the gate-channel capacitance, V_{GS} is the gate-source potential, U is the surface potential and q is the electronic charge. Because the technique offers previously unattainable resolution, it promises to yield new insights into electronic transport and degradation processes in organic semiconductors.

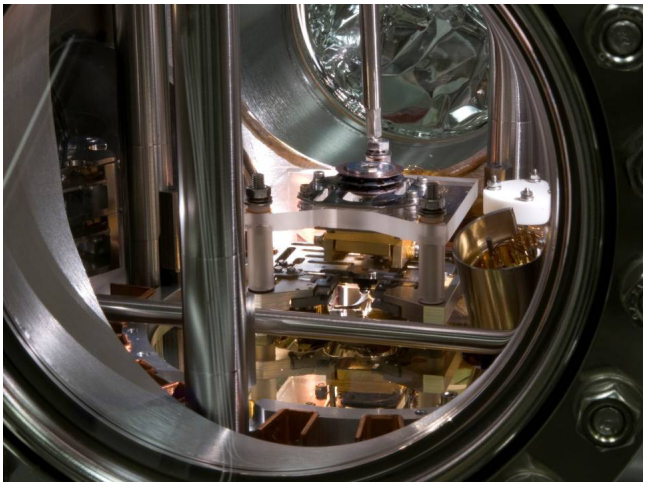

▲ Figure 1: Image of the VT-SPM (Omicron GmbH) inside the UHV chamber (3x10^{-10} Torr). Surface potential measurements are recorded relative to a Pt-Ir coated Si tip. Measurement of the tail states requires equilibrium in the channel. However, the resistance of the channel is extremely large below the threshold. Further measurements are required to determine whether the measurement of the extreme tail states have indeed been made under equilibrium conditions.

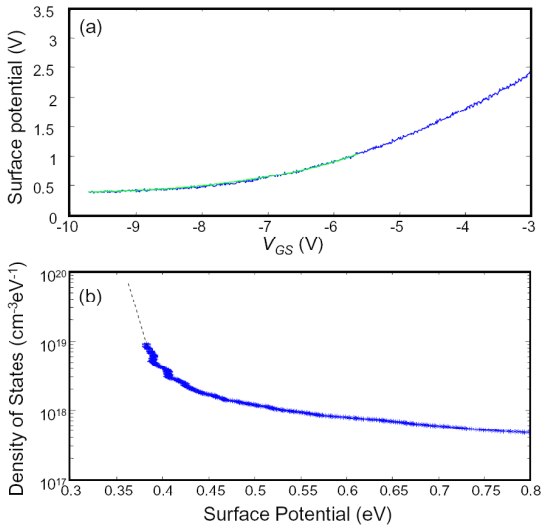

▲ Figure 2(a): The OFET channel surface potential versus the gate bias. The blue dots represent the actual data and the green line is a cosh-fit of the data. The OFET consists of 50-nm-thick Au top-contacts with a 50-μm-wide, 20-nm-thick CuPC channel on Si-substrate with 300-nm thermal oxide. (b) The calculated density of states noting that the measured density of the extreme tail states remains subject to additional verification.

REFERENCES

[1] M. Nonnenmacher, M.P. O'Boyle, and H. K. Wickramasinghe, "Kelvin probe force microscopy," *Applied Physics Letters*, vol. 58, pp. 2921-2923, June 1991.

[2] V. Palermo, M. Palma, and P. Samori, "Electronic characterization of organic thin films by Kelvin probe force microscopy," *Advanced Materials*, vol. 18, pp. 145-164, Dec. 2005.

[3] O. Tal, Y. Rosenwaks, Y. Preezant, N. Tessler, C.K. Chan, and A. Kahn "Direct determination of hole density of states in undoped and doped amorphous organic films with high lateral resolution," *Physical Review Letters*, vol. 95, pp. 256405:1-4, Dec. 2005.

Scanning Helium Ion Beam Lithography

B. Cord, M.K. Mondol, K.K. Berggren, L.A. Stern (Karl Zeiss SMT, Peabody, MA)

Scanning electron beam lithography (SEBL) has been the leading technology in low-volume, high-resolution nanofabrication for over three decades. Unfortunately inherent limitations of the technology, such as electron beam scattering, have made improvement in SEBL resolution past the 10-nanometer limit problematic. Recent advances in resist contrast enhancement have mitigated this somewhat, but reliable patterning of dense, sub-10-nm features remains nontrivial on even the most high-end SEBL tools.

One of the key advantages of patterning using a helium ion, rather than an electron beam, is the substantial reduction in beam scattering as it travels through the resist. Helium ions, with a comparatively higher mass, are affected much less by atomic collisions when traveling through a material and exhibit only minimal scattering in normal resist materials. Figure 1 shows the results of a Monte Carlo simulation of a 50 KeV helium ion beam traveling through a PMMA layer; at a depth of 50 nm (a typical resist thickness for many applications), the point-spread function of the beam is only 2 nm wide, narrower than even 100 KeV electron beams under similar conditions. This reduction in beam scattering should help reduce the proximity effect that makes patterning dense, high-resolution features difficult with SEBL.

Experimentation with helium ion beam lithography has recently been made possible by the development of a scanning helium ion beam microscope by Alis Corporation [1]. Their commercial-grade microscope has achieved imaging resolutions on the order of 1 nm, making it a promising candidate as a lithography tool. Basic experimentation with their lower-resolution "proof-of-concept" system has demonstrated that patterning and successful transfer of features is possible using standard SEBL processes. Figure 2 shows a field of Ti-Au dots patterned with the system using a film of PMMA on silicon and standard metallization and liftoff.

While issues such as vibration, pattern generation, and process control remain to be addressed, further experimentation with helium ion beam lithography may lead to a tool that meets or exceeds the performance of modern SEBL systems.

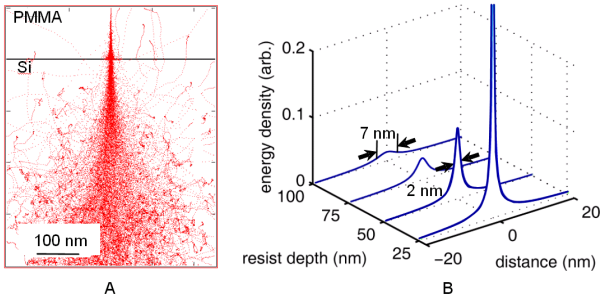

▲ Figure 1: Simulation of He ion scattering in resist. (a) Result of SRIM-based Monte Carlo simulation of ion-scattering for 50 keV He ions traveling through 100 nm of PMMA into a Si substrate (b) Analysis of the data from (a) showing how the distribution of deposited energy widens as a function of resist depth. After 50 nm of resist (a practical thickness to work with), the beam width is only 2 nm. Note that this model does not take secondary electrons generated by the ion beam into account, as the details of the ion-secondary electron interactions are not yet fully understood.

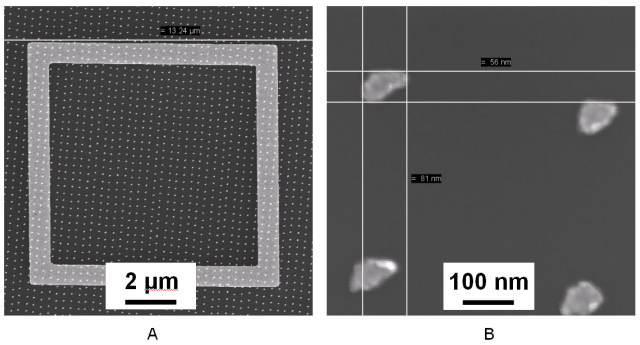

▲ Figure 2: Scanning electron micrographs of a field of Ti-Au dots at two magnifications, fabricated by exposing 90 nm PMMA on a Si substrate to a single raster-scan of a helium ion beam and performing metal evaporation and liftoff on the resulting pattern. The consistently irregular dot shape in (b) is thought to be the result of vibrations in the system. The large square in (a) is a previously-fabricated fiducial mark.

REFERENCES

[1] B.W. Ward, J.A. Notte, N.P. Economou, "Helium ion microscope: A new tool for nanoscale microscopy and metrology," *Journal of Vacuum Science and Technology B,* vol. 24, no. 6, pp. 2871-2874, Nov. 2006.

Nodal Optical Lithography: Breaking the Diffraction Limit

D. Winston, A. Chao, K. Rosfjord, S. Kooi, K. Berggren
Sponsorship: MIT, AFOSR

We propose to use the quantum-optical properties of materials to achieve super-resolution in optical lithography. By using beams of light instead of electrons, we can avoid substrate damage, use more intense fields that can write faster, and write with multiple beams simultaneously. By optically gating the photochemistry in the resist, we can squeeze the point-spread function of the resist exposure caused by the patterning pulse and thereby achieve sub-diffraction nanopatterning.

Resolution improvement in lithographic systems using the optical field nodes has already been demonstrated using nonlinear optical processes in neutral atoms [1]. The process used atoms in excited states and then de-excited the atoms before they were able to use their absorbed energy to stimulate a reaction. In the case of a photoresist, as was recently proposed [2], the goal is to de-excite the photo-initiating species before it can generate free radicals (Figure 1) and facilitate polymerization/crosslinking (in the case of negative-tone resist) or chain scission (in the case of positive-tone resist).

Arbitrary, dense patterning may be achieved using two synchronized laser pulses, the second of which is patterned so that it has at least one point of zero intensity, and a negative-tone resist with an appropriate photo-initiating species (Figure 2). Because the nodes – the points of zero intensity – in the second pulse determine the pattern transferred to the resist, we call this technique "nodal lithography." Increasing the intensity of the second pulse will "squeeze" the resulting pattern because even as pulse intensity rises, nodes remain nodes; herein lies the potential for diffraction-unlimited patterning.

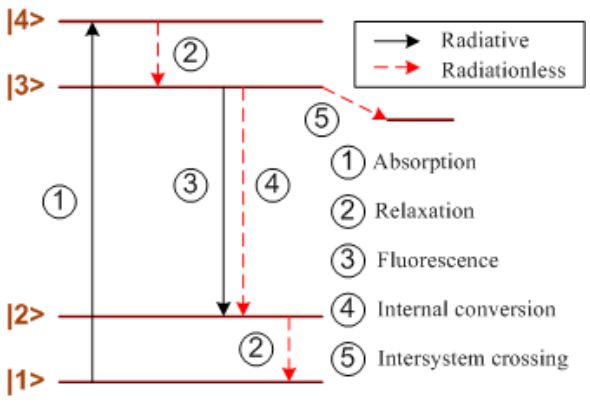

▲ Figure 1: Energy-level diagram that models a few of the photophysical transitions, both radiative and radiationless, that a fluorescent molecule can undergo upon absorption of light. Following absorption, chemical reactions will occur after intersystem crossing. Optical de-excitation would induce fluorescence before intersystem crossing, thus deactivating the resist and enabling a tighter point spread function for higher-contrast features.

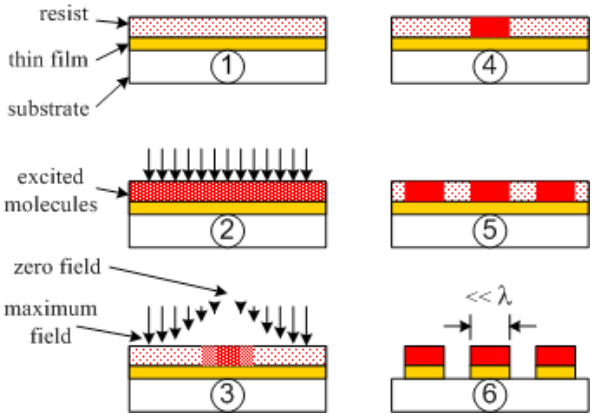

▲ Figure 2: Exposure sequence for nodal lithography with a single node: (1) a photolabile (resist) material is put on top of a film to be patterned; (2) the resist is excited uniformly, rendering it reactive; (3) the resist is selectively quenched by a patterned light; (4) the molecules near the node, which were not quenched in step (3), react; (5) the substrate is translated relative to the radiation and steps (2)-(4) are repeated to form an arbitrary pattern; (6) the resulting pattern is developed and then transferred to the underlying film using a chemical or physical etching process.

REFERENCES

[1] K.S. Johnson, J.H. Thywissen, N.H. Dekker, K.K. Berggren, A.P. Chu, R. Younkin, and M. Prentiss, "Localization of metastable atom beams with optical standing waves: nanolithography at the Heisenberg limit," *Science*, vol. 280, no. 5369, pp. 1583-6, June 1998.

[2] S.W. Hell, "Strategy for far-field optical imaging and writing without diffraction limit," *Physics Letters A*, vol. 326, no. 1-2, pp. 140-5, May 2004.

High-contrast Salty Development of Hydrogen Silsesquioxane

J.K.W. Yang, K.K. Berggren
Sponsorship: MIT

In electron-beam lithography (EBL), the highest resolution one can achieve depends primarily on the electron-beam spot size and the resist contrast. As the electron-beam spot size is constrained by the type of EBL system used, which is not easily modified, the only practical route to improved patterning resolution is to use resists with better contrast. Hydrogen silsesquioxane (HSQ) is a negative-tone electron resist that allows direct writing of etch-resistant silicon oxide nanostructures with low line-edge roughness. However, due to its low contrast, patterning high-resolution, densely packed nanostructures in HSQ has been a challenge. Recent efforts to increase the contrast of hydrogen silsesquioxane (HSQ) have focused on developing with more concentrated bases [1], and elevating development temperatures [2]. While these strong developers improve contrast, they also can cause material damage and are thus unsuitable in certain situations: for instance, hot or concentrated bases etch Si and hence are not compatible with Si processing.

In this work, we instead increased the contrast of HSQ by adding salt (NaCl) to an aqueous NaOH developer. Figure 1 shows contrast curves of HSQ using different amounts of salt in an aqueous solution of 1% wt NaOH. We noticed that the resist contrast increased with increasing amount of salt. For 4% wt NaCl in 1% wt NaOH, we demonstrated a contrast value of 10 with a 30 kV beam acceleration voltage exposure of a 120-nm-thick resist. This achieved contrast was more than triple those obtained from development in tetramethyl ammonium hydroxide (TMAH) [1,2]. We also notice that the addition of NaCl increased resist contrast without significant decrease in resist sensitivity. This effect allows one to achieve higher resolution without increasing electron-beam exposure times.

Finally, we studied the effect of development with salt on the fabrication of nanostructures. Figure 2 shows an SEM image of 13-nm-wide HSQ lines in a 30-nm-pitch grating. These gratings were formed by single-pass electron exposure of 50-nm-thick HSQ on Si at 30 kV acceleration voltage in a Raith 150 EBL system, followed by development in an aqueous solution of 1% wt NaOH with 4% wt NaCl for 4 mins. The addition of salt into the developer has enabled us to increase our resolution by roughly a factor of three. In addition to enhancing the contrast of HSQ, these experiments could provide an improved understanding of the developmental mechanism of HSQ.

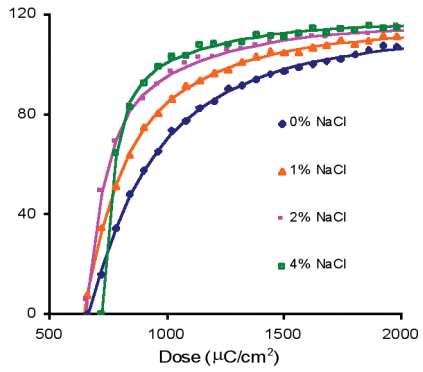

▲ Figure 1: Plot of remaining HSQ thickness vs. area dose for varying amounts of NaCl to aqueous 1% wt NaOH developer. Filled markers are data points while solid lines are fitting curves of exponential functions.

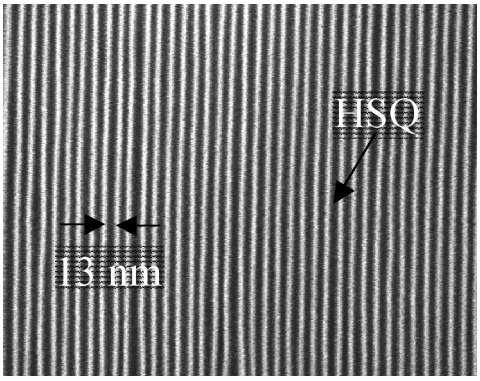

▲ Figure 2: An SEM micrograph of 13-nm-wide HSQ lines in a 30-nm-pitch grating on Si. Lines were exposed at 30 kV acceleration voltage and developed in 4% wt NaCl in 1% wt NaOH.

REFERENCES

[1] W. Henschel, Y.M. Georgiev, and H. Kurz, "Study of a high-contrast process for hydrogen silsesquioxane as a negative-tone electron-beam resist," *Journal of Vacuum Science & Technology B*, vol. 21, pp. 2018-2025, 2003.

[2] Y.F. Chen, H.F. Yang, and Z. Cui, "Effects of developing conditions on the contrast and sensitivity of hydrogen silsesquioxane," *Microelectronic Engineering*, vol. 83, pp. 1119-1123, 2006.

Templated Self-assembly of Sub-10-nm Quantum Dots

J. Leu, B. Cord, P. Anikeeva, M. Bawendi, V. Bulović, K.K. Berggren
Sponsorship: SRC/FCRP MSD

Patterned templates can guide the self-assembly of nanoparticles into ordered arrays [1]. Our motivation in pursuing templated self-assembly is to develop a robust method for the creation of ordered structures at length scales below ten nanometers. The basic process entails creating surface relief templates via electron-beam lithography and spin-coating a suspension of colloidal nanoparticles onto the template. The quantum dots self-assemble primarily through the capillary forces created by the dewetting of the template as the solvent evaporates [2].

We demonstrate this technique at sub-10-nm length scales by spin-coating a solution of organically capped semiconducting quantum dots onto nanopatterned grating structures on silicon substrates. We observe the geometric confinement of the quantum dots via physical templating and capillary forces into well-ordered monolayer aggregates with defined orientations. Additionally, we observe the presence of lattice strain in these aggregates, indicating the attractive interaction of the template with the quantum dots.

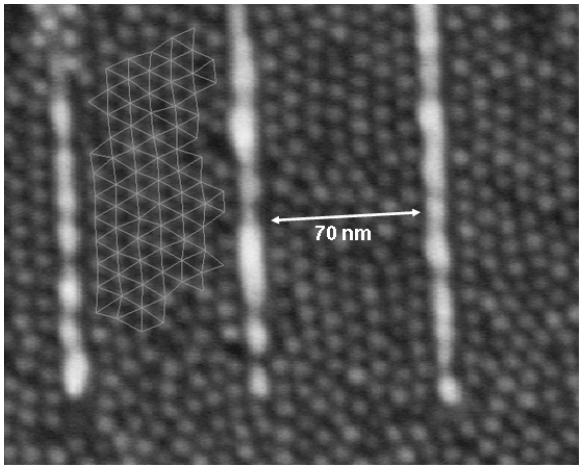

▲ Figure 1: Scanning electron micrograph of a self-assembled quantum dot monolayer on a templated silicon substrate. The vertical lines are part of a template grating, with 10-nm-wide, 80-nm-tall Au lines at a pitch of 80 nm. The spheres are organically capped 8-nm CdZnS semiconducting quantum dots. Shown superimposed on the image is a wire grid indicating the adjacency relations of a well-ordered aggregate.

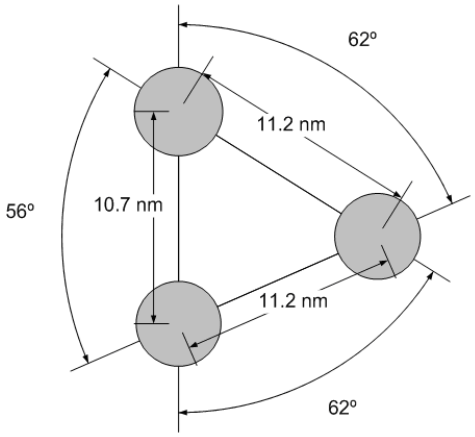

▲ Figure 2: The averaged center-to-center distances and orientation of the quantum dot aggregate highlighted in Figure 1. The direction of tensile strain is perpendicular to the grating lines.

REFERENCES

[1] Y. Yin, Y. Lu, B. Gates, and Y. Xia, "Template-assisted self-assembly: A practical route to complex aggregates of mondispersed colloids with well-defined sizes, shapes, and structures," *Journal of the American Chemical Society*, vol. 123, pp. 8718-8729, 2001.

[2] J.A. Liddle, Y. Cui, and P. Alivisatos, "Lithographically directed self-assembly of nanostructures," *Journal of Vacuum Science Technology B.*, vol. 22, no. 6, pp. 3409-3414, Nov./Dec. 2004.

Optical Properties of Superconducting Nanowire Single-photon Detectors

V. Anant, A.J. Kerman, J.K.W. Yang, E.A. Dauler, K.M. Rosfjord, K.K. Berggren
Sponsorship: AFOSR, Lincoln Laboratory, MIT

High-efficiency single-photon detection requires careful design of the device optics. For superconducting-nanowire single-photon detectors (SNSPDs) [1-3], this challenge is amplified by the complexities of optical propagation in subwavelength structures. We have conducted an initial theoretical study of the optical design issues that must be addressed to achieve efficient absorption of infrared light by SNSPDs. We found that the absorption depends not only on geometrical parameters of the device, but also on the polarization of the incident photon. We are now testing our model by directly measuring the optical absorptance of SNSPDs fabricated at MIT. We will then feed back the testing results to the design process to realize high-efficiency SNSPDs that, by design, are either sensitive or insensitive to incident photon polarization.

This work is sponsored by the United States Air Force under Air Force Contract #FA8721-05-C-0002. Opinions, interpretations, recommendations and conclusions are those of the authors and are not necessarily endorsed by the United States Government.

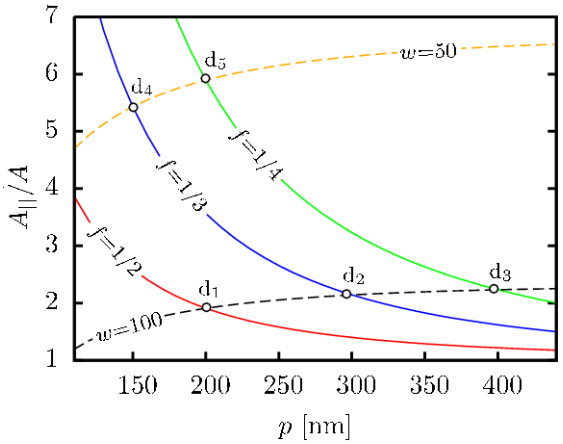

▲ Figure 1: Plot of the predicted ratio of parallel to perpendicular absorptance by the SNSPD as a function of pitch, *p*, wire width *w* (given in nm), and fill factor, *f=w/p*. A maximum sensitivity to polarization occurs when the fill factor and wire width are both small. We fabricated devices that correspond to points d_1-d_5 shown on this plot in order to test our model.

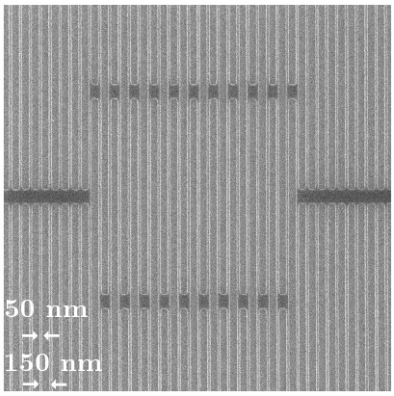

▲ Figure 2: Scanning electron micrograph of device d_4, where the wire width was 50 nm and pitch was 150 nm. This device was fabricated using processes described in [1] and tested using the apparatus described in [2] and [3].

REFERENCES

[1] J.K.W. Yang, E. Dauler, A. Ferri, A. Pearlman, A. Verevkin, G. Gol'tsman, B. Voronov, R. Sobolewski, W.E. Keicher, and K.K. Berggren, "Fabrication development for nanowire GHz-counting-rate single-photon detectors," *IEEE Transactions on Applied Superconductivity*, vol. 15, issue 2, part 1, pp. 626-630, June 2005.

[2] A.J. Kerman, E.A. Dauler, J.K.W. Yang, K.M. Rosfjord, V. Anant, G.N. Gol'tsman, B.M. Voronov, and K.K. Berggren, "Kinetic-inductance-limited reset time of superconducting nanowire photon counters," *Applied Physics Letters*, vol. 88, pp. 111116:1-3, Mar. 2006.

[3] K.M. Rosfjord, J.K.W. Yang, E.A. Dauler, A.J. Kerman, V. Anant, B.M. Voronov, G.N. Gol'tsman, and K.K. Berggren, "Nanowire single-photon detector with an integrated optical cavity and anti-reflection coating," *Optics Express*, vol. 14, issue 2, pp. 527-534, Jan. 2006.

Characterization of Nondegenerate Spontaneous Parametric Downconversion Photon-pair Sources Using a Superconducting Nanowire Single-photon Detector

X. Hu, A.J. Kerman, E. Dauler, J.K.W. Yang, A. Vikas, F.N.C. Wong, K.K. Berggren
Sponsorship: DTO, DARPA, MIT, AFOSR

As a basis of many quantum information processing applications, photon pairs can be generated efficiently by spontaneous parametric downconversion (SPDC) in a periodically poled lithium niobate (PPLN) crystal. For instance, pumped by a 532-nm laser source, the PPLN downconverter can efficiently yield nondegenerate photon pairs, a signal photon at ~800 nm and an idler photon at ~1600 nm [1]. To measure the efficiency of this process, we perform signal-idler coincidence measurements (Figure 1), which require high-efficiency, low dark-count-rate photon counters at those two wavelengths. To detect the signal photon at ~800 nm, a Si photon counter with efficiency about 50% is commercially available; however, to detect the idler photon at ~1600 nm, a commercial InGaAs avalanche photodiode (APD) can only achieve 20% detection efficiency.

We have instead fabricated a superconducting nanowire single-photon detector (SNSPD) to count the idler photons. Compared with the InGaAs APD, we have demonstrated that our SNSPD can achieve device detection efficiency as high as over 50% at near-infrared wavelengths [2]. Furthermore, to minimize the possible optical coupling loss from fiber to the SNSPD, we have designed an experimental setup to do optical coupling and helium-immersion SNSPD testing inside a dewar (Figure 2). We use a fiber focuser to shrink the mode size of the light down to 5-6 μm and a nanopositioner to further maximize the overlap of the optical mode and the SNSPD. Our preliminary calculation shows that our SNSPD can achieve ~50% system detection efficiency.

This work is sponsored by the United States Air Force under Air Force Contract #FA8721-05-C-0002. Opinions, interpretations, recommendations and conclusions are those of the authors and are not necessarily endorsed by the United States Government.

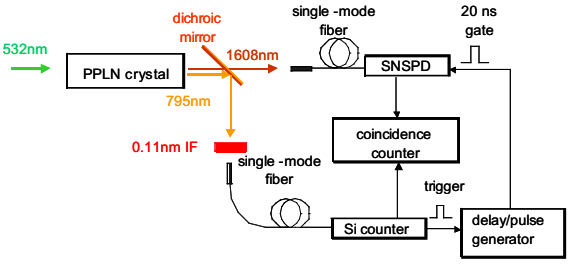

▲ Figure 1: Schematic for photon-pair generation and the signal-idler coincidence measurements.

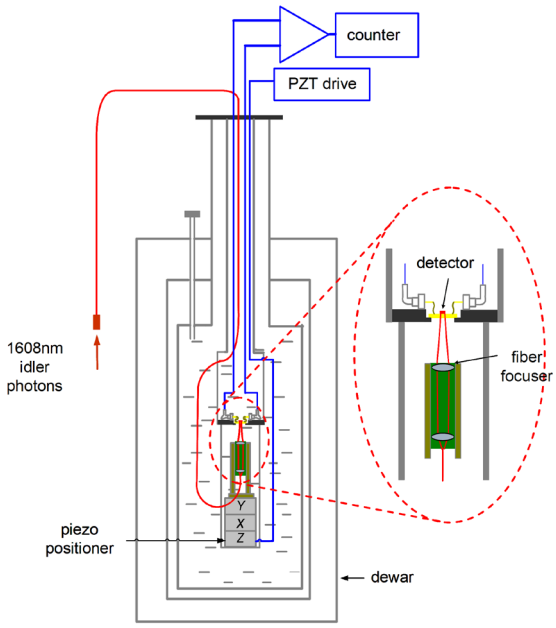

▲ Figure 2: Schematic for helium-immersion testing of superconducting nanowire single-photon detectors.

REFERENCES

[1] E.J. Mason, M.A. Albota, F. König, and F.N.C. Wong, "Efficient generation of tunable photon pairs at 0.8 and 1.6 μm," *Optics Letters*, vol. 27, no. 23, pp. 2115-2117, Dec. 2002.

[2] K.M. Rosfjord, J.K.W. Yang, E.A. Dauler, A.J. Kerman, V. Anant, B.M. Voronov, G.N. Gol'tsman, and K.K. Berggren, "Nanowire single-photon detector with an integrated optical cavity and anti-reflection coating," *Optics Express*, vol. 14, no. 2, pp. 527-534, Jan. 2006.

Micropatterning Organic Electronic Device Electrodes by PDMS Lift-off

J. Yu, V. Bulović
Sponsorship: PECASE, NSF MRSEC

Patterning of electrodes in organic electronic devices is done primarily by techniques that are limited in resolution and scalability or are potentially damaging to the underlying organic material. We demonstrate a subtractive stamping technique for patterning the top metal electrode of organic electronic devices. Patterning is achieved by placing a relief-patterned polydimethylsiloxane (PDMS) stamp in contact with a metal electrode and quickly peeling off the stamp (Figure 1a). The fast peel rate increases the adhesion energy of the PDMS to the metal electrode, allowing the stamp to pick up the metal from the substrate.

The in-plane roughness of the patterned straight edge is less than 1 um (Figure 1b) while the transition region of the patterned abrupt step is less than 0.1 um in width (Figure 1c). We pattern micron-sized features on a glass substrate with an ITO step with good yield (Figure 2). We have shown that for organic light emitting devices, this technique is comparable to the traditional shadow masking technique [1]. This technique can also be applied to patterning gold electrodes for organic pentacene transistors.

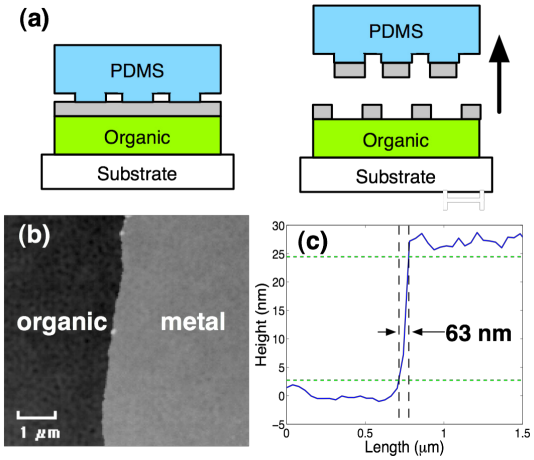

▲ Figure 1: (a) Demonstration of the subtractive stamping technique. A quick release of the PDMS stamp to the substrate is required to lift off metal film from substrate surface. (b) Top view of in-plane roughness of patterned edge of organic to metal from AFM (c) AFM height data to view transition region of organic to metal edge.

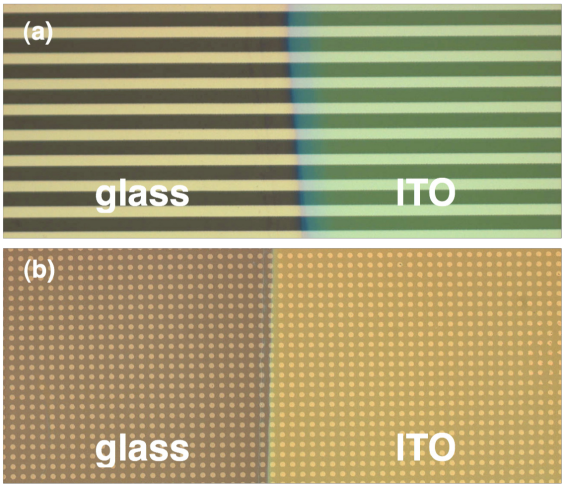

▲ Figure 2: Optical microscope image of (a) 13-um-wide lines patterned from 17-nm-thick Mg:Ag film and (b) 25-um-diameter circles on 11-nm-thick Mg:Ag film on top of 50-nm Alq3, 50-nm TPD, 40-nm PEDOT, and 80-nm ITO or glass substrate. Both images show the technique can work even on a step of ITO on a glass substrate.

REFERENCES

[1] J. Yu and V. Bulović, "Patterning nicron-sized features of quantum dots and metal electrodes," Massachusetts Institute of Technology, Cambridge, MA, Microsystems Technology Laboratory Annual Research Report, 2006.

Microcontact Printing of Quantum-dot LEDs Using an Inkjet-assisted Patterning Method

J. Yu, J. Chen, H. Huang, M. Bawendi, V. Bulović
Sponsorship: PECASE, NSF MRSEC, Hewlett-Packard

Colloidal quantum dots (QDs) with tunable emission wavelength, narrow emission band and efficient luminescence have been incorporated into OLEDs and used as lumophores in the QD-LED structure. In the past, the favored method of QD deposition has included a spin-coating step that does not utilize most of the QD material [1-2]. We propose an alternative method that directly patterns the QD layers on a stamp by inkjet printing and is subsequently transferred onto organic material via microcontact printing (Figure 1a). This technique allows patterning of the QD material and drastically improves material usage in fabrication of QD-LEDs and other optoelectronic devices that utilize QD thin films.

With a thermal inkjet printer from Hewlett Packard, we pattern QDs onto a polydimethylsiloxane (PDMS) stamp with a feature size of 50μm. Interaction between the QD solution and the stamp surface plays an important role in the formation of the inkjet printed QD patterns. Coating the stamp with a layer of parylene allows for better drying properties of the ink on the stamp (Figure 1b). The QD patterns have been transfer stamped onto organic hole transport layers (Figure 2a). The QD-LED structure is completed by subsequent deposition of a hole blocking layer, electron transport layer, and electrode, and electroluminescence images of QD-LEDs are shown in Figure 2b and c.

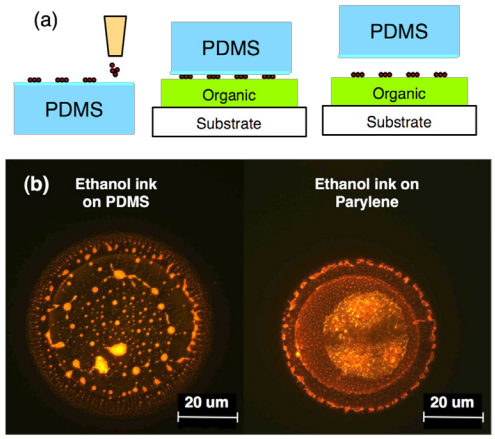

▲ Figure 1: (a) Inkjet printed quantum-dot technique (b) Photoluminescence of quantum-dot drop on different stamp surfaces.

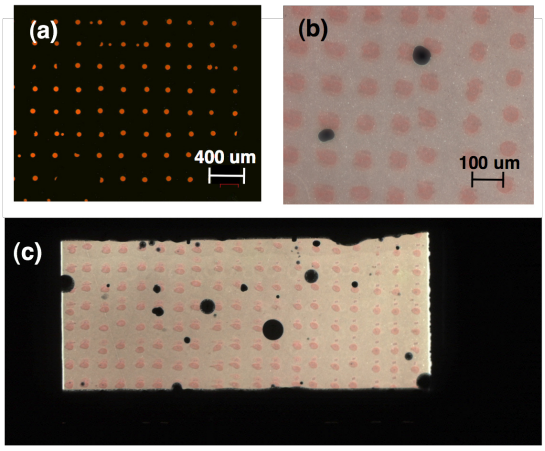

▲ Figure 2: (a) Photoluminescence of inkjet printed red quantum dots transfer printed from parylene coated PDMS stamp to TPD. (b) and (c) Electroluminescence from an inkjet-assisted patterned QD-LED.

REFERENCES

[1] S. Coe-Sullivan, J. Steckel, W. Woo, M. Bawendi, and V. Bulović, "Large-area ordered quantum-dot monolayers via phase separation during spin-casting," *Advanced Functional Materials*, vol. 15, no. 7, pp. 1117-1124, July 2005.

[2] L. Kim, "Deposition of colloidal quantum dots by microcontact printing for LED display technology," Master's thesis, Massachusetts Institute of Technology, Cambridge, MA, 2006.

Electronic and Excitonic Processes in Quantum Dot LEDs

P.O. Anikeeva, C.F. Madigan, J.E. Halpert, M.G. Bawendi, V. Bulović
Sponsorship: ISN, NSF MRSEC, PECASE

Hybrid light emitting devices (LEDs) based on organic charge transporting materials and emissive colloidal quantum dot monolayers have demonstrated superior color purity and high external quantum efficiency close to that of organic LEDs (OLEDs) [1], making them a technology that can potentially replace OLEDs in flat panel displays. While fabrication methods for QD-LEDs have been extensively studied over the past several years, the mechanisms of QD-LED operation still present a significant scientific challenge. Understanding the excitonic and electronic processes in QD-LEDs is crucial to efficient device design.

We investigate the mechanism of operation of the hybrid organic/colloidal quantum dot (QD) light emitting devices (QD-LEDs). By varying the position of the emitting QD monolayer within the stacked organic structure, we find that the quantum efficiency of the device improves by >50% upon imbedding the emissive QD monolayer into the hole-transporting layer <10 nm below the interface between hole and electron transporting layers. We analyze these results in the context of two different mechanisms for QD light emission: the charge injection model and the exciton energy transfer model. We find that maximizing energy transfer contribution to QD luminescence improves QD-LED performance, primarily due to inefficiencies arising from charged QDs.

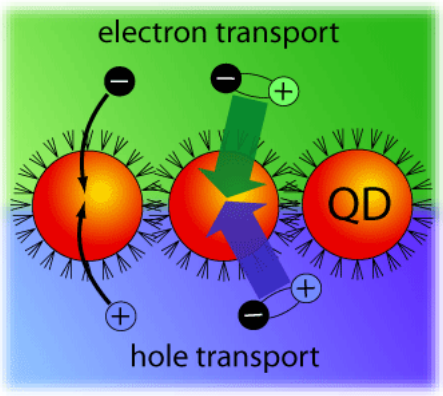

▲ Figure 1: Schematic diagram of the charge injection and energy transfer from organic charge transporting layers to a monolayer of colloidal CdSe/ZnS core-shell QDs.

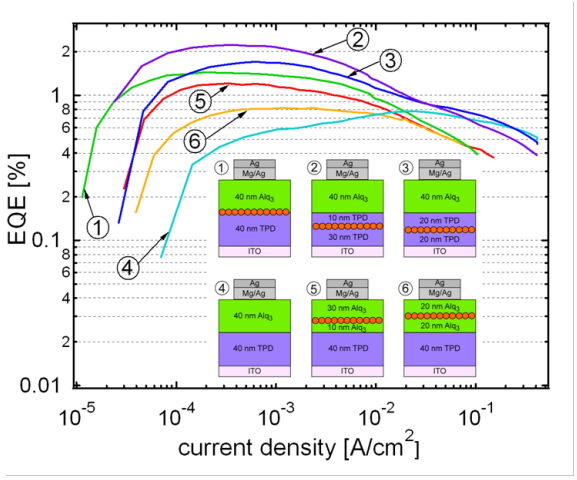

▲ Figure 2: External quantum efficiency curves are shown for six devices displayed in the inset. The highest EQE of 2.3% corresponds to the device 2, in which a QD monolayer is imbedded 10 nm into TPD layer below the TPD/Alq$_3$ interface.

REFERENCES

[1] S.A. Coe-Sullivan, "Hybrid organic/quantum dot thin film structures and devices," Ph.D thesis, Massachusetts Institute of Technology, Cambridge, MA, 2005.

[2] L. Kim, "Deposition of colloidal quantum dots by microcontact printing for LED display technology" M. Eng. thesis, Massachusetts Institute of Technology, Cambridge, MA, 2006.

Förster Energy Transfer from Fluorescent and Phosphorescent Organic Small Molecules to J-aggregate Thin Films

Y. Shirasaki, P.O. Anikeeva, J.R. Tischler, M.S. Bradley, V. Bulović
Sponsorship: ISN, NSF MRSEC, PECASE

Due to their extremely narrow absorption spectra and high peak absorption constant (α~1.0x10 cm), J-aggregated thin films composed of the anionic cyanine dye TDBC electrostatically adsorbed to the cationic polyelectrolyte PDAC (poly diallyldimethylammonium chloride) present an interesting material for thin film opto-electronic devices. For example, J-aggregated film was successfully incorporated into a microcavity light-emitting device (LED) to produce strongly coupled states of light and matter [1]. Its strong dipole also enables us to consider its application as an efficient light-harvesting material that can transfer energy to other materials of interest, such as quantum dots.

As an initial step in this research, we study Förster resonance energy transfer (FRET) from fluorescent (Alq_3) and phosphorescent ($Ir(ppy)_3$) donors to the J-aggregated films. The two donor materials were chosen for the large overlap between their emission spectra and J-aggregate absorption spectrum, allowing for efficient long range (~10nm) FRET. In order to find a Förster radius and potentially a magnitude of the J-aggregate transition dipole, an organic spacer layer of high bandgap material (TAZ) with varying thickness of 0-15 nm with 3 nm increments is deposited between the acceptor and donor films. The donor films are excited with a 400-nm pulsed laser and the total photon emission from the films is measured using a streak camera as shown in Figure 1. Figure 2 shows the J-aggregate photoluminescence decay times changing with respect to the distance to the donor film, indicating an efficient FRET.

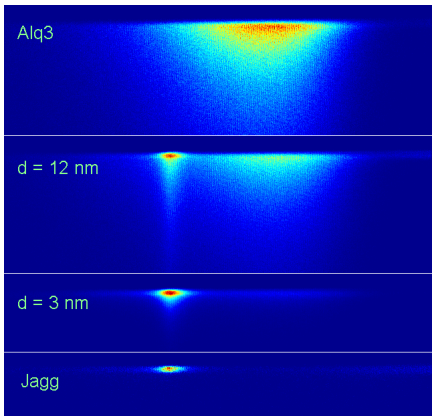

▲ Figure 1: Streak camera pictures of photon emission from films with the J-aggregate (acceptor) and Alq_3 (donor) layers with varying spacer layer thickness d in between.

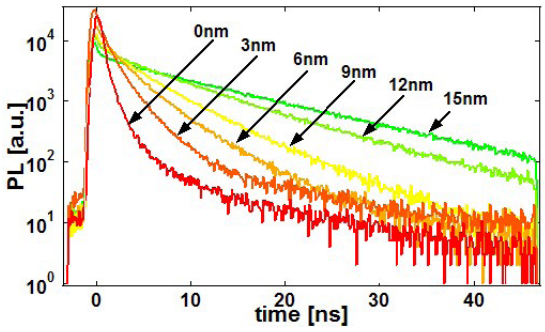

▲ Figure 2: Time-resolved PL measurements of J-aggregate emission from films with Alq_3 as the donor material. The spacer layer thicknesses between the donor and the acceptor layers vary from 0-15 nm with 3 nm increments.

REFERENCES

[1] Tischler, J.R., M.S. Bradley, V. Bulović, J.H. Song, and A. Nurmikko, "Strong coupling in a microcavity LED," *Physical Review Letters*, vol. 95, pp. 36401:1-4, July 2005.

Combined Impact of Field and Carrier Concentration on Charge- carrier Mobilities in Amorphous Organic Thin Films

C. Madigan, V. Bulović

We report Monte Carlo (MC) simulations of charge-carrier transport in amorphous organic solids and provide the first calculations of the field-dependent charge-carrier mobility in the presence of elevated carrier concentrations in energetically disordered solids. We utilize the Miller-Abrahams field-assisted hopping rate [1] to perform mobility calculations over a range of carrier concentrations, electric fields and energy disorders typically encountered in organic electronic devices. We find that charge accumulation in energetically disordered solids increases the mobility, with the strongest effects at the lowest applied fields and the highest energy disorders. We show that the Poole-Frenkel regime [2-3] persists at elevated carrier concentrations. However, comparison of our MC calculations shows that existing analytic theory of charge transport in amorphous solids [4] inadequately accounts for impact of carrier concentration on charge transport as it neglects hopping cycles and improperly uses Fermi statistics under non-equilibrium conditions.

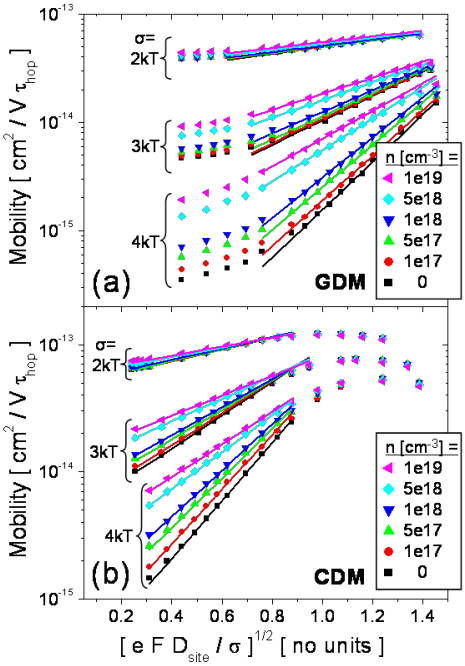

▲ Figure 1: Equilibrium mobility as a function of field and carrier concentration, n, subject to two Gaussian disorder models (GDM and CDM) for σ = [2-4] k_BT.

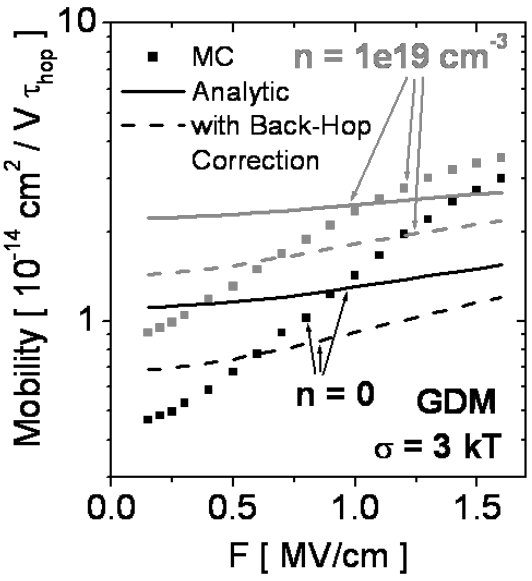

▲ Figure 2: Comparison of equilibrium mobility as computed by MC calculations and existing analytic theory [4] for the GDM with σ = 3 k_BT.

REFERENCES

[1] A. Miller and E. Abrahams, "Impurity conduction at low concentrations," *Physical Review*, vol. 120, p. 745, June 1960.
[2] J. Frenkel, "On pre-breakdown phenomena in insulators and electric semi-conductors," *Physical Review*, vol. 54, p. 647, Oct. 1938.
[3] D.M. Pai, "Transient photoconductivity in poly(N-vinylcarbazole," *Journal of Chemical Physics*, vol. 52, pp. 2285-2291, Mar. 1970.
[4] Y. Roichman, Y. Presszant, and N. Tessler, "Analysis and modeling of organic devices," *physica status solidi (a)*, vol. 201, pp. 1246-1262, May 2004.

Ambient Environmental Patterning of Organic Thin Films by a Second-generation Molecular Jet (MoJet) Printer

J. Chen, V. Leblanc, P. Mardilovich, M.A. Schmidt, V. Bulović
Sponsorship: Hewlett-Packard

Organic light emitting device (OLED) technology for use in flat panel display (FPD) applications would benefit greatly from the development of a reliable, repeatable, additive patterning technique of forming organic electroluminescent (EL) thin films. We previously demonstrated that the first-generation molecular jet (MoJet-I) printing technique is superior to the two industrial mainstream methods to pattern the EL layers, namely shadow-masking patterning for molecular organics and InkJet printing for polymeric materials [1-2]. We present here the concept and application of the second generation (MoJet-II) printing technique. Using an improved silicon MEMS printhead, we demonstrate the feasibility of ambient environmental patterning of molecular organic EL thin films directly by local evaporative deposition. Three stages are involved in the printing process. In the first stage, thermal InkJet printing technology is used to dispense ink drops into a micro-machined silicon membrane consisting of an array of 8 by 8 micro-pores and an integrated heater. Once the pores are filled, in the second stage, a small current is passed through the heater to completely drive off solvent from the micro-pores. In the final stage, a pulsed current of larger magnitude is applied to heat up the pores to a temperature sufficient to discharge the dry ink materials out of the pores and form molecular flux. The flux is then condensed onto a nearby substrate, forming designated thin-film EL patterns.

MoJet printing combines the advantages of the film purity of thermally evaporated films with the flexibility of direct patterning to enable "flux on demand" deposition of molecular organic thin films with scalability over arbitrary form/size substrates. Such ambient environmental patterning can enable high-quality, low-cost, on-demand digital fabrication of organic devices [3].

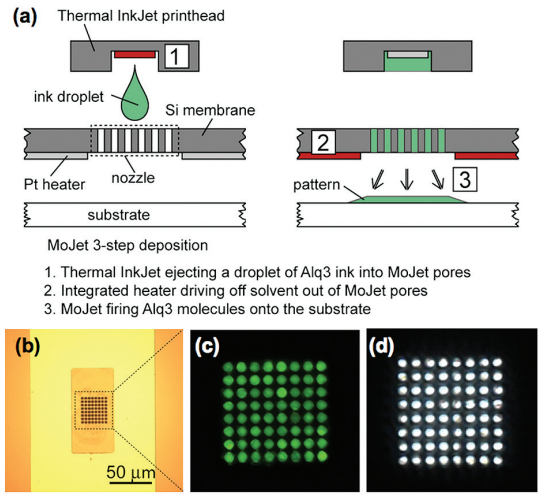

▲ Figure 1: (a) Schematic diagram of MoJet-II 3-step deposition; (b) MoJet-II printhead; (c) Photoluminescent (PL) image of printhead micro-pores filled with ink; (d) Empty pores after printing, ready for the next round of receiving ink.

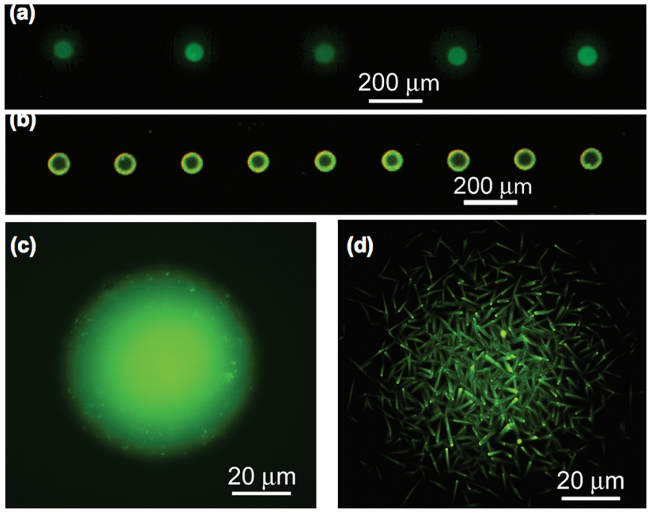

▲ Figure 2: MoJet-II printing results (a) in comparison with the inkjet printing results (b) with identical ink composition; (c) Individual OLED pixel reveals improved thickness uniformity under PL excitation; (d) example of the final printed pattern annealed by excessive solvent.

REFERENCES

[1] S.R. Forrest, "The path to ubiquitous and low-cost organic electronic appliances on plastic," *Nature*, vol. 428, p. 911, Apr. 2004 .

[2] V. Leblanc, J. Chen , S.H. Kang, V. Bulović, and M.A. Schmidt, "Micromachined Printheads for the Evaporative Patterning of Organic Materials and Metals," *J. of Microelectromech. Syst.*, vol.16, p. 394, 2007.

[3] J. Chen, V. Leblanc, P. Mardilovich, M.A. Schmidt, and V. Bulović, "Evaporative deposition of molecular organics in ambient with a molecular jet printer," *International Conference on Digital Fabrication Technologies*, Sept. 2006.

Heterojunction Photovoltaics Using Printed Colloidal Quantum Dots as a Photosensitive Layer

A.C. Arango, D.C. Oertel, M.G. Bawendi, V. Bulović
Sponsorship: ISN

Colloidal quantum dot (QD) systems offer distinct optical and electronic properties that are not easily attained by other nanostructured semiconductors, such as highly saturated emission in QD light-emitting-diodes, access to infrared radiation in QD photodetectors, and the prospect of optically optimized solar cell structures. The prevailing deposition method for colloidal QD systems is spin casting, which introduces limitations such as solvent incompatibility with underlying films and the inability to pattern side-by-side pixels for multispectral photodetector arrays. In the present work we employ a non-destructive microcontact printing method, which allows for deposition of a thin quantum dot films onto a wide-band-gap organic hole transport layer, N,N'-bis-(3-methylphenyl)-N,N'-bis-(phenyl)-benzidine (TPD), thus producing an inorganic/organic heterojunction that serves to enhance charge separation in the device. The top and bottom contacts are provided by ITO electrodes, allowing for near transparency.

We observe a photocurrent spectrum that follows the QD absorption profile. The magnitude of the quantum efficiency is low, due in part to minimal absorption and also to excess charge transport losses in the CdSe layer. We achieve a maximum short circuit current density at a QD film thickness corresponding to 3% absorption. By changing the size and material properties of the QDs, the response spectrum of the device can be tuned across visible and near infra-red. The present focus is on improving the device's performance and optimizing the photodetection response in the 1μm to 2μm wavelength region by utilizing different QD film chemistries.

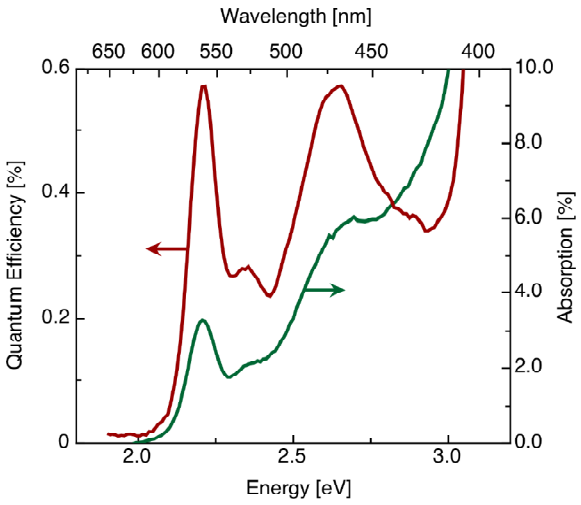

▲ Figure 1: Plot of the quantum efficiency and absorption versus incident photon energy and wavelength. The absorption is determined by measuring the transmission and reflection of the entire device stack. The internal quantum efficiency at the first absorption peak is 16%..

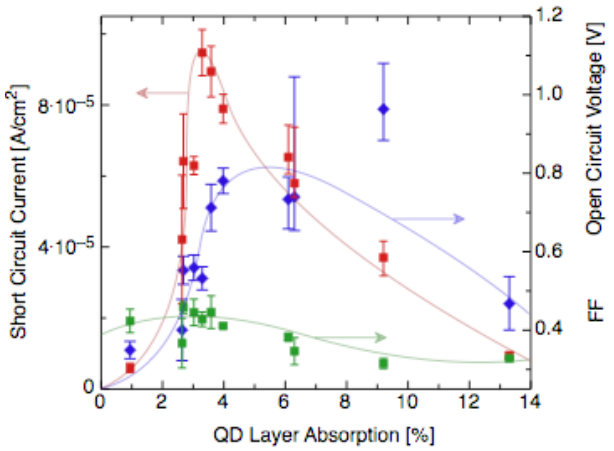

▲ Figure 2: Plot of the short circuit current, open circuit voltage and fill factor (FF) for devices where the QD layer thickness is varied from greater than six monolayers (13% absorption) to less than complete surface coverage (1% absorption). Lines are guides to the eye.

REFERENCES

[1] D.C. Oertel, M.G. Bawendi, A.C. Arango, and V. Bulović. "Photodetectors based on treated CdSe quantum-dot films," *Applied Physics Letters*, vol. 87, no. 21, pp. 213505:1-3, Nov. 2005.

Transmission and Flux Due to Surface Phonon-Polaritons

D.-Z. A. Chen, A. Narayanaswamy, X. Chen, G. Chen (in coll. with R. Hamam, M. Soljačić, J.D. Joannopoulos)
Sponsorship: DOE, MURI (through UC Berkeley)

Surface phonon-polaritons are electromagnetic surface waves that are present in dielectrics with a negative permittivity. These near-field modes lead to interesting far-field phenomena such as extraordinary optical transmission through sub-wavelength holes. Although light propagation is classically cut-off by the holes, experimental Fourier transform infra-red measurements of the transmission through the perforated film show that significant transmission still occurs [1]. As shown in Figure 1, the enhanced transmission occurs only for certain frequency ranges. Furthermore, these frequencies correspond exactly with where surface phonon-polaritons are found and are also confirmed by finite-difference time-domain simulations.

The in-plane thermal conductivity due to surface phonon-polaritons has also been examined. The in-plane energy transfer due to these surface polaritons is modeled as a diffusive process in an absorbing medium. Due to the well-known very long propagation length of the anti-symmetric mode, it was found that the surface polaritons can make a significant contribution to the effective thermal conductivity along thin films. In particular, for a 50-nm-thick film of amorphous silicon dioxide, the total thermal conductivity was calculated to be 4 W m^{-1} K^{-1} at 500K, which is an increase of ~100% over the intrinsic phonon thermal conductivity [2], as shown in Figure 2.

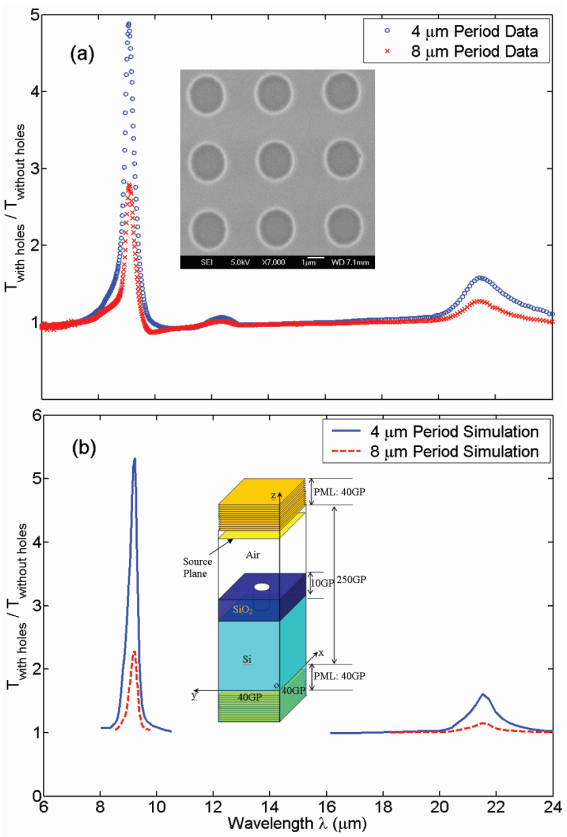

▲ Figure 1: Transmission through silicon dioxide films perforated with 2-μm holes normalized to the transmission through a solid film. (a) The experimentally measured transmission spectra. The inset shows a scanning electron micrograph of the actual sample. (b) FDTD simulation results for the same structures. The inset shows a schematic of the computational cell for the structure with a 4-μm period.

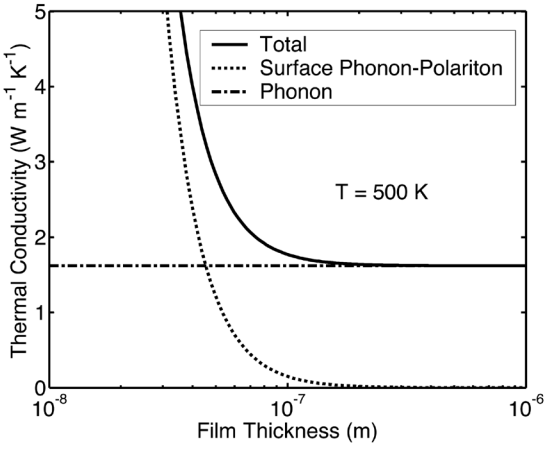

▲ Figure 2: Amorphous silicon dioxide (glass) thermal conductivity due to phonons and surface phonon-polaritons as a function of film thickness at 500 K.

REFERENCES

[1] D.-Z. A. Chen, R. Hamam, M. Soljačić, J. D. Joannopoulos, and G. Chen, "Extraordinary optical transmission through sub-wavelength holes in a polaritonic silicon dioxide film," *Applied Physics Letters*, vol. 90, no. 18, pp. 181921:1-3, Apr. 2007.

[2] D.-Z. A. Chen, A. Narayanaswamy, and G. Chen, "Surface phonon-polariton mediated thermal conductivity enhancement of amorphous thin films," *Phys. Rev. B*, vol. 72, no. 15, pp. 155435:1-4, Oct. 2005.

High-throughput, Continuous-flow Separation of Biomolecules in a High-aspect-ratio Nanofilter Array

P. Mao, J. Han
Sponsorship: KIST IMC, NSF

We have developed a novel fabrication approach to generate massively-parallel, high-aspect-ratio vertical nanofluidic channels with smooth, vertical sidewalls and precise control of uniform gap sizes (lateral trench width) down to 50 nm (Figure 1) [1]. The aspect ratio can be as high as 400 and the channel depths are more than 20 μm. This technique enables us to fabricate a large area of solid membrane structures with well-defined pore size and geometries, which can be very useful for membrane-based application such as filtration, separation and fuel cells. Also, using such systems as molecular sieving filters, we demonstrated efficient continuous-flow size-fractionation of large DNA molecules in a two-dimensional (2D) vertical nanofilter array device fabricated by this method (Figure 2). Our device allows much higher sample volume processing rate (1μL/hour), compared with the planar nanofilter array chip previously reported [2]. We believe that these devices could be a key to the efficient proteomic sample preparation microsystems as well as useful in purifying and separating various bioparticles and nanoparticles.

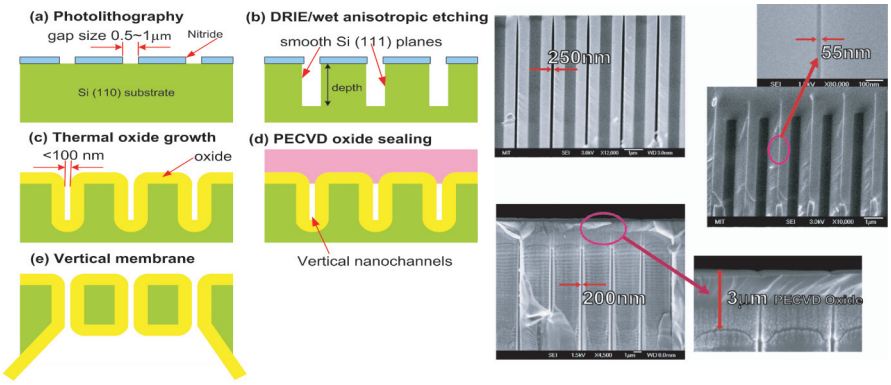

▲ Figure 1: (A) Schematic diagram of fabricating massively-parallel vertical nanofluidic membranes. (B) Cross-sectional SEM micrograph of vertical nanochannels with lateral gap sizes (widths) of 250 nm, 200 nm, and 30 nm.

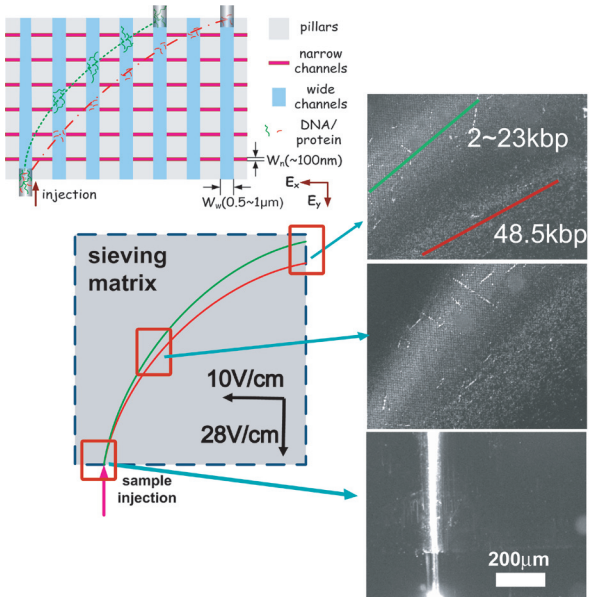

▲ Figure 2: Bidirectional transport of molecules (top view) and fluorescence micrographs of continuous fractionation of the mixture of λ-DNA and λ-DNA Hind III digest in 2D vertical nanofilter array device. Electrical fields in both horizontal and longitudinal directions are applied over the sieving matrix. The gap sizes (widths) of horizontal and longitudinal channels are around 100 nm and 500 nm, respectively.

REFERENCES

[1] P. Mao and J. Han, "Fabrication and characterization of planar nanofluidic channels and massively-parallel nanofluidic membranes," presented at *Proc. of the μTAS 2005 Symposium*, Oct. 2005.

[2] J. Fu and J. Han, "A nanofilter array chip for fast gel-free biomolecule separation," presented at *Proc. of the μTAS 2005 Symposium*, Oct. 2005.

Transplanting Assembly of Single-strand Carbon Nanotubes

S. Kim, H.W. Lee, S.G. Kim
Sponsorship: Intelligent Microsystems Center

Most of the potential applications of carbon nanotubes (CNTs) such as field emitters, scanning probe microscopy (SPM) tips, and nanowire interconnection require deterministic assembly techniques with control of shape (diameter and length), orientation, location, and range. We are developing a new deterministic assembly method for single strand CNTs such that the individual CNTs can be integrated into micro-scale devices. For this purpose, we propose and demonstrate a concept of transplanting assembly of individual CNTs. An array of nickel catalytic dots is seeded at the predefined locations on a titanium deposited silicon wafer using electron beam lithography followed by a metal liftoff process. An array of vertically aligned CNTs is grown from the Ni catalysts (Figure 1) using plasma enhanced chemical vapor deposition (PECVD) machine developed by Micro & Nano Systems Laboratory of MIT [1-2]. Each single strand CNT is embedded into polymer blocks, which work as CNT carriers. A 1.5-μm-thick positive photoresist is coated on the silicon wafer before 20-μm-thick negative photoresist (SU8 of MicroChem Corp.) is coated on top of it. The SU8 layer is patterned into cylindrical blocks. Finally, each SU8 block encapsulating one single-strand CNT is released by removing the positive photoresist layer (Figure 2). Each released SU-8 block can be transplanted to the location of interest using the assembly methods readily available at the micro scales.

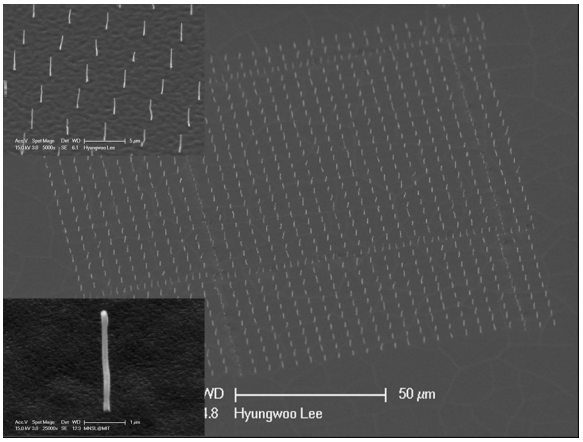

▲ Figure 1: An array of vertically aligned single strand CNTs. CNTs were grown straight on the seeded area, and the enlarged view shows that each CNT has a uniform diameter from the top to the bottom.

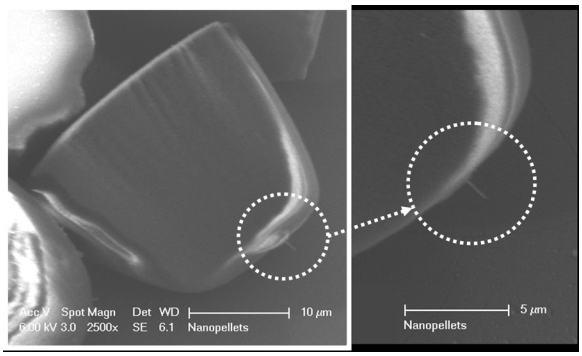

▲ Figure 2: An SU8 block with a single CNT on one side. The length of the extruded CNT is 1.5μm, and this is the same as the thickness of the positive photoresist layer.

REFERENCES

[1] T. El-Aguizy, J.H. Jeong, Y.B. Jeon, W.Z. Li, Z.F. Ren and S.G. Kim, "Transplanting carbon nanotubes," *Appl. Phys. Lett,* vol. 85, no. 25, p. 5995, Dec. 2004.

[2] C. Mueller-Falcke, S.D. Gouda, S. Kim, and S.G. Kim, "A nanoscanning platform for bio-engineering: In-plane probe for switchable stiffness," *Nanotechnology,* vol. 17, pp. S69-S76, Jan. 2006.

Growth Mechanisms of Horizontally Aligned Carbon Nanotubes by CVD

A. Reina, M. Hofmann, D. Zhu, J. Kong
Sponsorship: SRC/FCRP IFC, Intel Higher Education Program

The selective production of long, horizontally aligned carbon nanotubes (>1mm) or short, randomly oriented carbon nanotubes (<50μm) was achieved in a chemical vapor deposition process by influencing the catalyst pretreatment and reaction conditions. A detailed investigation was undertaken to elucidate the mechanism yielding the two different morphologies. It was found that the duration of the catalytic growth of a nanotube plays a vital role; i.e., the actual growth period of long nanotubes is significantly higher (up to 15 minutes or more) compared to short nanotubes (10 seconds or less). Alignment with the gas flow occurs only when a nanotube reaches a critical length, which suggests that short growth durations limit not only the length of CNTs but also their alignment with the gas flow. Furthermore, it is concluded that differences in the nanoparticle's catalytic lifetime is the most probable factor determining the extension of growth duration and lengths to obtain long, horizontally aligned CNTs. This work represents a step forward towards the integration of CNTs in electronic applications.

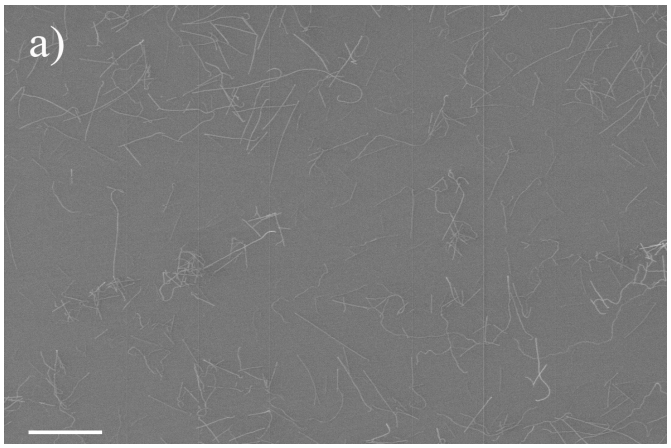

▲ Figure 1: An SEM micrograph of short, randomly aligned carbon nanotubes.

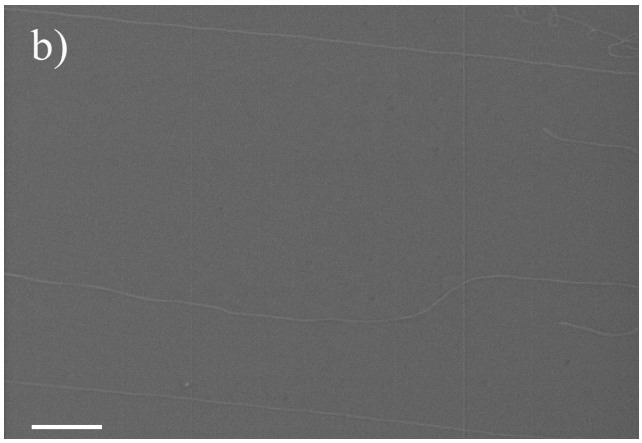

▲ Figure 2: An SEM micrograph of long, gas-flow-aligned carbon nanotubes.

REFERENCES

[1] A. Naeemi, R. Sarvari, and J.D. Meindl, "Performance comparison between carbon nanotube and copper interconnects for gigascale integration (GSI)," *IEEE Electron Device Letters*, vol. 26, no. 2, pp. 84-86, Feb. 2005.

[2] M. Moniruzzaman, and K.I. Winey, "Polymer nanocomposites containing carbon nanotubes," *Macromolecules*, vol. 39, no. 16, pp. 5194-5205, Aug. 2006.

[3] B.H. Hong, J.Y. Lee, T. Beetz, Y.M. Zhu, P. Kim, and K.S. Kim, "Quasi-continuous growth of ultralong carbon nanotube arrays," *Journal of the American Chemical Society*, vol. 127, no. 44, pp. 15336-15337, Nov. 2005.

[4] S.M. Huang, M. Woodson, R. Smalley, and J. Liu, "Growth mechanism of oriented, long single-walled carbon nanotubes using 'fast-heating' chemical vapor deposition process," *Nano Letters* vol. 4, no. 6, pp. 1025-1028, June 2004.

[5] L.X. Zheng, M.J. O'Connell, S.K. Doorn, X.Z. Liao, Y.H. Zhao, E.A. Akhadov, M.A. Hoffbauer, B.J. Roop, Q.X. Jia, R.C. Dye, D.E. Peterson, S.M. Huang, J. Liu, and Y.T. Zhu, "Ultralong single-wall carbon nanotubes," *Nature Materials*, vol. 3, no. 10, pp. 673-676, Oct. 2004.

Templated Assembly by Selective Removal

M. Hyers, F. Eid, C. Livermore
Sponsorship: NSF Career Award, Pappalardo Fellowship, NSF Graduate Research Fellowship

Templated assembly by selective removal (TASR) is an effective technique for site-selective multi-component assembly at the nano- and micro-scales. In this project, the TASR approach has been created and quantitatively modeled; work to expand the technology and demonstrate practical applications is now underway. The TASR approach offers great promise for assembling arbitrary (not necessarily periodic) systems of multiple different types of nanoscale components, such as electronics and biological or chemical sensing devices. It also offers a path to a new kind of shape and size selective chromatography.

The key elements of the approach follow. First, the topography of the substrate is modified to match the components' 3D shapes. Then the substrate and components are coated with an adhesion promoter, such as a hydrophobic SAM for adhesion in a water-based environment. The components and substrate are placed in a fluid environment for the assembly process, and megahertz frequency ultrasound is applied to the fluid bath. Components contact the substrate randomly and adhere wherever they land; however, components that are not in shape-matched sites are removed by fluid force, which is initiated by the high-frequency ultrasound. The fluid forces create a moment that rolls components from mismatched holes. Components in shape-matched sites are selectively retained because the adhesive forces create a stronger moment that retains components in matching holes. Figure 1 is an optical micrograph showing the successful assembly of 600-nm- and 2-mm-diameter silica microspheres into designated sites on the substrate. The TASR approach has been demonstrated for component sizes down to about 400 nm and with a variety of excitation and interaction strengths. Figure 2 shows how the assembly yield (the ratio of the number of filled sites to the total number of sites) varies with the ratio of the retention moment to the removal moment.

This approach to assembly is inherently selective; since each component will adhere only in a shape- and size-matched site, geometrically distinct components will assemble only into their designated assembly sites. The TASR method allows the organizing information to be stored in the template initially and permits components that may not be compatible with top-down manufacturing techniques to be added to the system later, with high positional precision. Present work is focused on the creation of improved models based on molecular dynamics simulations, extension of TASR to smaller size scales and a diverse set of component shapes and materials, and improved template fabrication techniques, with the goal of demonstrating practical applications enabled by the TASR approach.

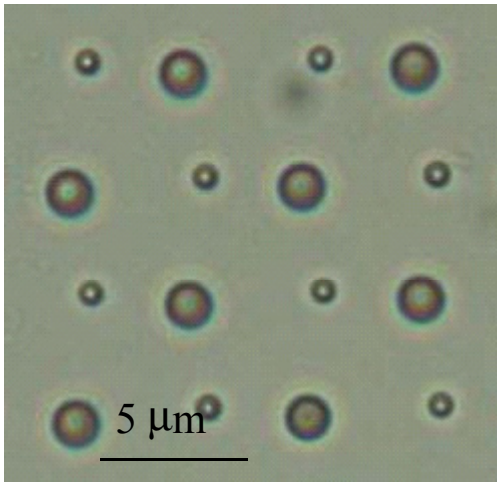

▲ Figure 1: Optical micrograph of a template with assembled spheres of two different sizes.

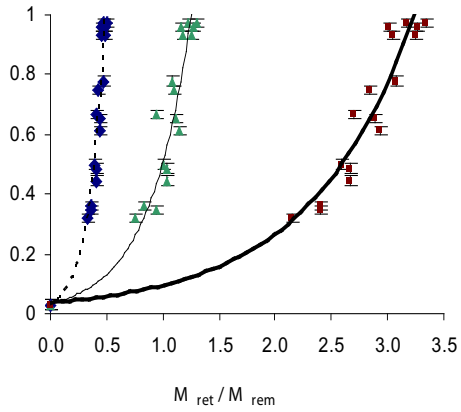

▲ Figure 2: Plot of yield versus retention to removal moment ratio for the simultaneous assembly of 636-nm- and 2-µm-diameter spheres with various excitation and interaction strengths. The plot shows the actual data points and the fitted curves for the cases of minimum, nominal, and maximum moment ratios.

REFERENCES

[1] S. Jung and C. Livermore, "Achieving selective assembly with tem-plate topography and ultrasonically induced fluid forces," *Nano Letters*, vol. 5, no. 11, pp. 2188-2194, Nov. 2005.

Templated Self-assembly of Block Copolymers for Nanolithography

C.A. Ross, H.I. Smith, F. Ilievski, V. Chuang, Y.S. Jung
Sponsorship: NSF, CMSE, Singapore-MIT Alliance, SRC

By combining "bottom-up" self-assembly with "top-down" patterned templates, templated self-assembly can provide many advantages in nanofabrication methods. Block copolymers consist of two covalently bound polymer chains of chemically distinct polymer materials. The chains can self-assemble to form small-scale domains whose size and geometry depend on the molecular weights of the two types of polymer and their interaction [1]. Previously, sphere-forming polystyrene-b-ferrocenyldimethylsilane (PS-PFS) diblock copolymers were successfully aligned in 2-D [2] or 3-D [3] templates. On the one hand, with the purpose of fabricating arrays of magnetic nanosized dots, we are working on templating the block copolymers in a removable template. These arrays are a potential candidate for magnetic hard-drive media, but the flexibility of the technique allows it to be extended to the fabrication of other devices such as plasmon waveguides or biomedical devices. On the other hand, cylindrical morphology of block copolymers can be used for defining nanoscale line patterns. Poly(styrene-b-dimethylsiloxane) (PS-PDMS) diblock copolymers have a large interaction parameter between two blocks, which is desirable for long-range ordering [4]. The high density of Si in the backbone of PDMS provides extremely high etch contrast between the two blocks when it is treated in an oxygen plasma, which is advantageous for pattern transfer into underlying materials. The cylinders can be oriented either parallel (Figure 1) or perpendicular (Figure 2) to the template by controlling mesa width and solvent vapor pressure. Beyond rather limited morphologies of diblock copolymers, an appropriate combination of block sequence, interaction parameter of the adjacent blocks, volume fraction, and molecular weights of ABC triblock polymer thin films provides a diversity of new structures. For example, a concentric cylinder forming triblock polymer thin films can be used as a lithographic mask for patterning a magnetic film into rings via an etching process. As shown in Figure 3, a concentric forming PB-PS-PMMA is vertically oriented after solvent annealing.

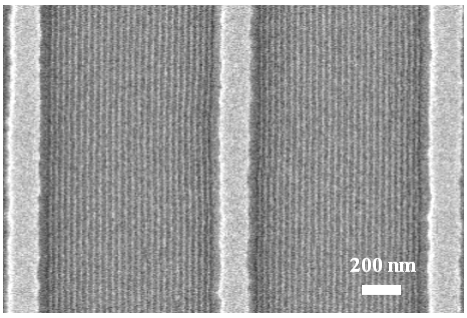

▲ Figure 1: Parallel cylinders from PS-PDMS diblock copolymers on trench substrates.

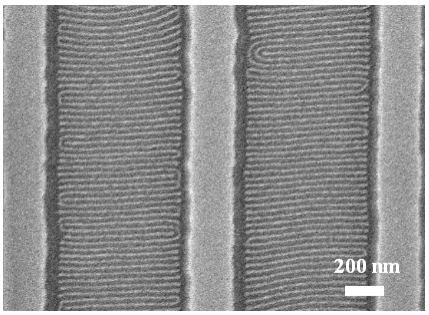

▲ Figure 2: Perpendicular cylinders from PS-PDMS diblock copolymers on trench substrates.

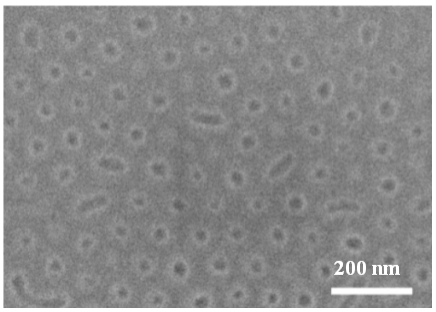

▲ Figure 3: Vertically oriented hollow cylinders of PS. The PMMA at the center of the cylinders and PB matrix are partly removed.

REFERENCES

[1] E.L. Thomas, R.L. Lescanec *et al.*, "Phase morphology in block copolymer systems," *Phil. Trans. R. Soc. Lond. A*, vol. 348, no. 1686, pp.149-166, July 1994.

[2] J. Cheng, C.A. Ross, and A. Mayes, "Nanostructure engineering by templated self-assembly," *Nature Materials*, vol. 3, pp. 823-828, Oct. 2004.

[3] V.P. Chuang, J.Y. Cheng, T.A. Savas, and C.A. Ross, "Three-dimensional self-assembly of spherical block copolymer domains into V-shaped grooves," *Nano Letters*, vol. 6, pp. 2332 -2337, Oct. 2006.

[4] Y.S. Jung and Caroline A. Ross, "Orientation-controlled Self-assembled Nanolithography using a Polystyrene-Polydimethylsiloxane Block Copolymer," *Nano Letters*, vol. 7, no. 7, pp. 2046-2050, July 2007

Scanning Beam Interference Lithography

M. Ahn, C.-H. Chang, R. Heilmann, Y. Zhao, M.L. Schattenburg
Sponsorship: NASA, Plymouth Grating Laboratory

Traditional methods of fabricating gratings, such as diamond tip ruling, electron and laser beam scanning, or holography, are generally very slow and expensive and result in gratings with poor control of phase and period. More complex periodic patterns, such as gratings with chirped or curved lines or 2D and 3D photonic patterns, are even more difficult to pattern. This research program seeks to develop advanced interference lithography tools and techniques to enable the rapid patterning of general periodic patterns with much lower cost and higher fidelity than current technology.

Interference lithography (IL) is a maskless lithography technique based on the interference of coherent beams. Interfering beams from an ultra-violet laser generates interference fringes, which are captured in a photo-sensitive polymer resist. Much of the technology used in modern IL practice is borrowed from technology used to fabricate computer chips. Traditional IL methods result in gratings with large phase and period errors. We are developing new technology based on interference of phase-locked scanning beams, called scanning beam interference lithography (SBIL). The SBIL technique has been realized in a tool called the MIT Nanoruler, which recently won an R&D 100 award (Figure 1). Large gratings can be patterned in a matter of minutes with a grating phase precision of only a few nanometers and a period error in the ppb range (Figure 2).

Current research efforts seek to generalize the SBIL concept to pattern more complex periodic patterns, such as variable period (chirped) gratings, 2D metrology grids, and photonic patterns [1]. Important applications of large, high-fidelity gratings are for high-resolution x-ray spectroscopes on NASA x-ray astronomy missions, high-energy laser pulse-compression optics, and length metrology standards. We are in the process of a major upgrade of the Nanoruler optical and mechanical system that will allow rapid variation and control of grating pitch and fringe orientation, which will enable a new mode of operation of the Nanoruler that we call variable-period SBIL.

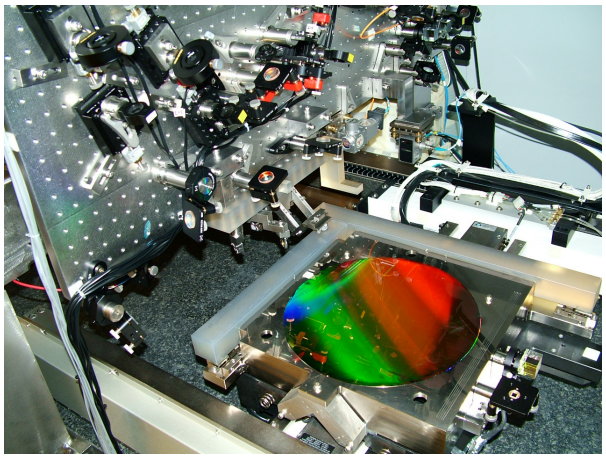

▲ Figure 1: Photograph of the Nanoruler lithography and metrology system built by MIT students. This unique tool is the most precise grating patterning and metrology system in the world.

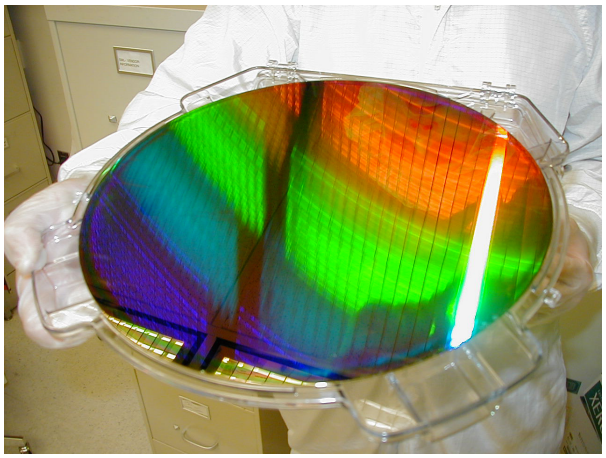

▲ Figure 2: A 300-mm-diameter silicon wafer patterned with a 400-nm-period grating by the Nanoruler. The grating is diffracting light from the overhead fluorescent bulbs.

REFERENCES

[1] G.S. Pati, R.K. Heilmann, P.T. Konkola, C. Joo, C.G. Chen, E. Murphy, and M.L. Schattenburg, "A generalized scanning beam interference lithography system for patterning gratings with variable period progressions," *Journal of Vacuum Science Technology B*, vol. 20, pp. 2617-2621, Nov. 2002.

[2] P. Konkola, C. Chen, R.K. Heilmann, C. Joo, J. Montoya, C.-H. Chang and M.L. Schattenburg, "Nanometer-level repeatable metrology using the Nanoruler," *Journal of Vacuum Science Technology B*, vol. 21, pp. 3097-3101, Nov. 2003.

[3] J. Montoya, C.-H. Chang, R.K. Heilmann and M.L. Schattenburg, "Doppler writing and linewidth control for scanning beam interference lithography," *Journal of Vacuum Science Technology B*, vol. 23, pp. 2640-2645, Nov. 2005.

[4] C.-H. Chang, R.K Heilmann and M.L. Schattenburg, "Advanced heterodyne fringe-locking system using multiple frequency shifts," *Proc. of the 20th Annual Meeting of the American Society for Precision Engineering*, vol. 37, pp. 375-378, Oct. 2005.

Nanometrology

R. Heilmann, Y. Zhao, D. Trumper, M.L. Schattenburg
Sponsorship: NSF

Manufacturing of future nanodevices and systems will require accurate means to pattern, assemble, image and measure nanostructures. Unfortunately, the current state-of-the-art of dimensional metrology, based on the laser interferometer, is grossly inadequate for these tasks. While interferometers can be very precise when used in carefully-controlled conditions, they typically have an accuracy measured in microns rather than nanometers. Achieving high accuracy requires extraordinarily tight control of the environment and thus high cost. Manufacturing at the nanoscale will require new technology for dimensional metrology that enables sub-1 nm precision and accuracy in realistic factory environments.

A recently formed MIT–UNC-Charlotte team is developing new metrology technology based on large-area grating patterns that have long-range spatial-phase coherence and ultra-high accuracy. Our goal is to reduce errors in gratings by 10-100 times over the best available today. These improved gratings can be used to replace interferometers with positional encoders to measure stage motion in new nanomanufacturing tools and to calibrate the dimensional scales of existing nanofabrication tools. This increased precision and accuracy will enable the manufacturing of nanodevices and systems that are impossible to produce today. Improved dimensional accuracy at the nano-to-picometer scale will have a large impact in many nanotechnology disciplines including semiconductor manufacturing, integrated optics, precision machine tools, and space research.

As part of this effort, we will utilize a unique and powerful tool recently developed at MIT called the Nanoruler that can rapidly pattern large gratings with a precision well beyond other methods. Another unique high-precision tool, the UNCC-MIT-built Sub-Atomic Measuring Machine (SAMM), is being brought to bear to research new ways to quantify and reduce errors in the gratings. Recent work at MIT is focused on improving the thermal controls in the Nanoruler lithography enclosure and developing an improved interferometer system to reduce errors in the stage metrology frame. At UNCC the SAMM is undergoing extensive refurbishment and improvements designed to boost interferometer accuracy.

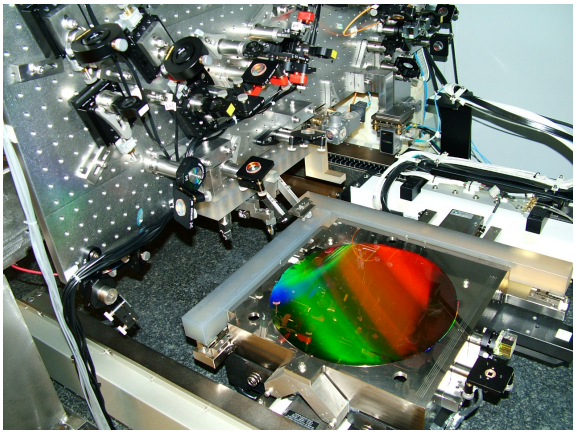

▲ Figure 1: Photograph of the Nanoruler lithography and metrology system built by MIT students. This unique tool is the most precise grating patterning and metrology system in the world.

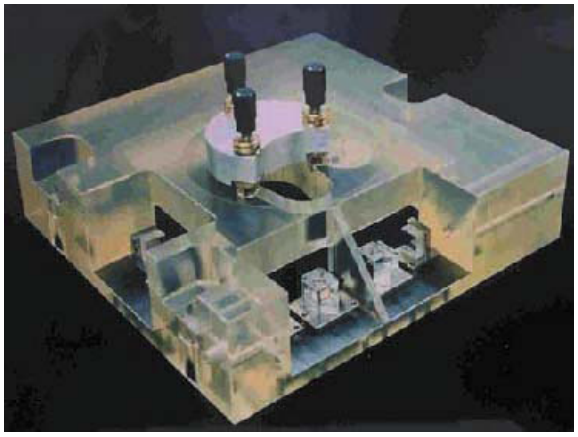

▲ Figure 2: Photograph of reference block/sample holder for the Sub-atomic Measuring Machine at the University of North Carolina at Charlotte.

REFERENCES

[1] P. Konkola, C. Chen, R.K. Heilmann, C. Joo, J. Montoya, C.-H. Chang, and M.L. Schattenburg, "Nanometer-level repeatable metrology using the Nanoruler," *Journal of Vacuum Science Technology B*, vol. 21, pp. 3097-3101, Nov. 2003.

[2] R.K. Heilmann, C.G. Chen, P.T. Konkola, and M.L. Schattenburg, "Dimensional metrology for nanometer-scale science and engineering: towards sub-nanometer accurate encoders," *Nanotechnology*, vol. 15, pp. S504-S511, Oct. 2004.

[3] J. Montoya, R.K. Heilmann, and M.L. Schattenburg, "Measuring two-axis stage mirror non-flatness using linear/angular interferometers," *Proc. of the 19th Annual Meeting of the Amer. Soc. for Precision Engineering*, vol. 34, pp. 382-385, Oct. 2004.

[4] Y. Zhao, C.-H. Chang, J. Montoya, R.K. Heilmann, and M.L. Schattenburg, "Measurement of milli-degree temperature gradients in environmental enclosures," *Proc. of the 20th Annual Meeting of the Amer. Soc. for Precision Engineering*, vol. 37, pp. 226-229, Oct. 2005.

Nanofabricated Reflection and Transmission Gratings

M. Ahn, C.-H Chang, R.K. Heilmann, Y. Zhao, M.L. Schattenburg
Sponsorship: NASA

Diffraction gratings and other periodic patterns have long been important tools in research and manufacturing. Diffraction occurs due to the coherent superposition of waves—a phenomenon with many useful properties and applications. Waves of many types can be diffracted, including visible and ultraviolet light, x-rays, electrons and even atom beams. Periodic patterns have many useful applications in fields such as optics and spectroscopy, filtering of beams and media, metrology, high-power lasers, optical communications, semiconductor manufacturing, and nanotechnology research in nanophotonics, nanomagnetics and nanobiology.

The performance of a grating is critically dependant on the geometry of individual grating lines. Lines can have rectangular, triangular or other geometries, depending on the application. High efficiency requires control of the geometric parameters that define individual lines (e.g., width, height, smoothness, sidewall angle, etc.) in the nanometer or even sub-nanometer range. For some applications, control of grating period in the picometer to femtometer range is critical. Traditional methods of fabricating gratings, such as diamond tip ruling, electron and laser beam scanning, or holography, generally result in gratings that fall far below theoretical performance limits due to imperfections in the grating line geometry. The main goal of our research is to develop new technology for the rapid generation of general periodic patterns with control of geometry measured in the nanometer to sub-nanometer range in order to achieve near-theoretical performance and high yields.

Fabrication of gratings is generally accomplished in two main steps, (1) lithographic patterning into a photosensitive polymer resist, followed by (2) pattern transfer. A companion research program in this report entitled *Scanning Beam Interference Lithography* describes progress in advanced grating patterning. In this abstract we report on research in pattern transfer technology. Development of a variety of grating geometries and materials is ongoing. Advanced gratings have been fabricated for 10 NASA missions, and further advances are sought for future missions [1]. Figure 1 depicts a gold wire-grid transmission grating designed for filtering deep-UV radiation for atom telescopes, while Figure 2 depicts a nano-imprinted saw-tooth reflection grating for x-ray spectroscopy.

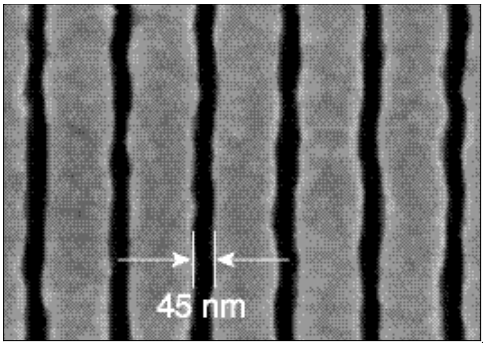

▲ Figure 1: Scanning-electron micrograph of a deep-UV blocking grating used in atom telescopes on the NASA *IMAGE* and *TWINS* missions. The grating blocks deep-UV radiation while passing energetic neutral atoms.

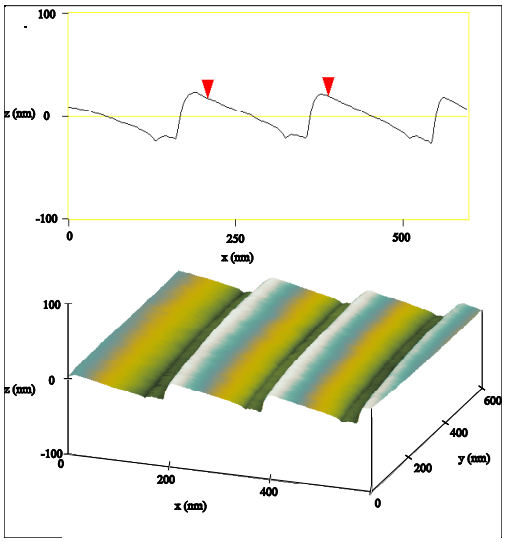

▲ Figure 2: An AFM image of 200-nm-period nano-imprint grating with 7° blaze angle developed for the NASA *Constellation-X* mission. The groove surfaces are extremely smooth, with an RMS surface roughness of <0.2 nm.

REFERENCES

[1] M.L. Schattenburg, "From nanometers to gigaparsecs: the role of nanostructures in unraveling the mysteries of the cosmos," *Journal of Vacuum Science Technology B,* vol. 19, no. 6, pp. 2319-2328, Nov. 2001.

[2] C.-H. Chang, R.K. Heilmann, R.C. Fleming, J. Carter, E. Murphy, M.L. Schattenburg, T.C. Bailey, R.D. Frankel, and R. Voisin, "Fabrication of saw-tooth diffraction gratings using nanoimprint lithography," *Journal of Vacuum Science Technology B,* vol. 21, no. 6, pp. 2755-2759, Nov. 2003.

[3] C.-H. Chang, J.C. Montoya, M. Akilian, A. Lapsa, R.K. Heilmann, M.L. Schattenburg, M. Li, K.A. Flanagan, A.P. Rasmussen, J.F. Seely, J.M. Laming, B. Kjornrattanawanich and L.I. Goray, "High-fidelity blazed grating replication using nanoimprint lithography," *Journal of Vacuum Science Technology B,* vol. 22, no. 6, pp. 3260- 3264, Nov. 2004.

[4] M.P. Kowalski, R.K. Heilmann, M.L. Schattenburg, C.-H. Chang, F.B. Berendse and W.R. Hunter, "Near-normal-incidence extreme-ultraviolet efficiency of a flat crystalline anisotropically etched blazed grating," *Applied Optics* vol. 45, no.8, pp. 1676-1679, Mar. 2006.

[5] J.F. Seely, L.I. Goray, B. Kjornrattanawanich, J.M. Laming, G.E. Holland, K.A. Flanagan, R.K. Heilmann, C.-H. Chang, M.L. Schattenburg, and A.P. Rasmussen, "Efficiency of a grazing-incidence off-plane grating in the soft x-ray region," *Applied Optics,* vol. 45, no. 8, pp. 1680-1687, Mar. 2006.

Microscale Single-Chamber Solid Oxide Fuel Cell Stacks

E.J. Crumlin, G.J. la O', Y. Shao-Horn
Sponsorship: GEM, MIT-Lemelson Fund, Ford-MIT Alliance, NSF MRSEC

Solid oxide fuel cells (SOFCs) are electrochemical conversion devices that convert various fuel sources directly into electrical energy at temperatures ranging from 600 to 1000°C. These high temperatures could potentially allow the direct use of various hydrocarbon fuel sources and hydrogen, without the need for expensive noble metal catalyst. Conventional SOFCs are designed in a two-chamber system, separating the fuel and oxidant flow to the anode and cathode, respectively. However, fuel cell manufacturing cost and robustness has proven to be the main challenge to rapid commercialization. A promising alternate method to achieve these requirements and to open up new architecture designs for the SOFC is the single-chamber solid oxide fuel cell (SC-SOFC). The SC-SOFC avoids many of manufacturing challenges associated with conventional SOFCs and has shown optimal performance between 500 and 800°C. Figure 1 demonstrates how a SC-SOFC operates. This device reduces the need for high temperature sealing and a complicated manifold structure; however, it also reduces the partial pressure of the gases at the electrodes, which reduces the theoretical obtainable voltage.

The architecture of a SC-SOFCs allows for entire fuel cells to be manufactured with a micro-size scale. Figure 2 shows the manufacturing processes to create micro SC-SOFCs. After successfully fabricating these micro SC-SOFCs, the fuel cells are tested in a microprobe station with a custom gas chamber enclosure. Current micro SC-SOFCs using Au and Pt electrodes are among the smallest created and obtain an OCV of 0.4V and a power density of approximately 0.03mW/cm^2. The OCV is comparable to previous studies[1]; however, the power is much lower due to the non-porous electrodes and thin electrolyte layers.

Future research will involve characterizing micro SC-SOFCs to understand the fundamental reaction mechanisms, electrode materials, and architectures to obtain dense, high performing stacks of micro SC-SOFCs.

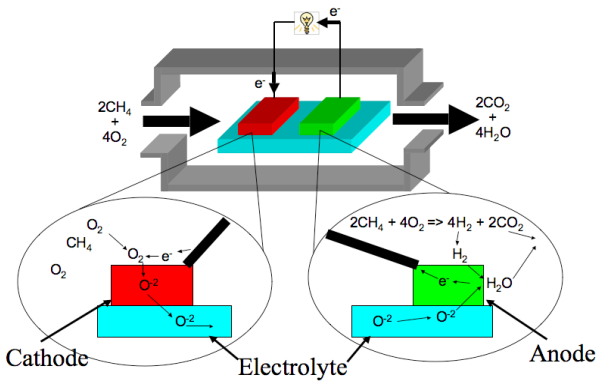

▲ Figure 1: The diagram depicts how a SC-SOFC works; the kinetic reactions are driven by the selective reactions that occur at each electrode. The cathode will selectively reduce oxygen to form an oxygen anion, which traverses the electrolyte to the anode. The anode selectively breaks down the fuel into hydrogen atoms, which lose an electron (to flow through the electrical circuit providing electrical power then to the cathode to create the oxygen anions) to form a proton that combines with the oxygen anion from the cathode, thus creating water molecules and completing the electrochemical reaction.

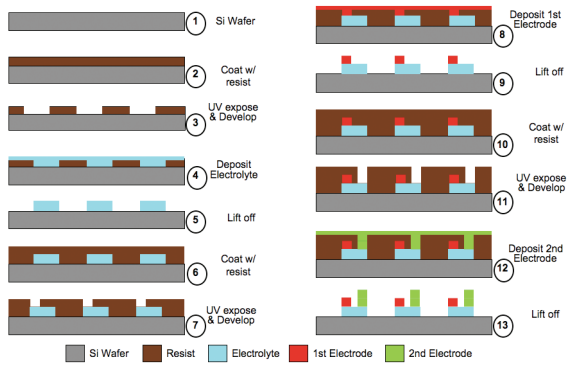

▲ Figure 2: This schematic depicts the fabrication steps used to produce micro-sized SC-SOFCs: (1) a silicon wafer is used as the SC-SOFC support; (2) a spin-coating of negative photoresist is applied; (3) photo-mask with electrolyte features; (4) 8YSZ is deposited by sputtering for 2 hours; (5) excess 8YSZ is lifted off by removing the resist with a photoresist stripper, leaving the desired electrolyte features; (6) photoresist is applied; (7) photo-mask with the first electrode features is exposed; (8) Au is deposited via sputtering; (9) excess Au is lifted off; (10) photoresist; is applied (11) photo-mask with the second electrode features is exposed; (12) Pt is deposited via sputtering; (13) excess Pt is lifted off, completing the micro SC-SOFC.

REFERENCES

[1] Ahn, S.-J., J. Moon, J.-H. Lee, and J. Kim, "Single-chamber solid oxide fuel cell with micro-patterned interdigitated electrodes," *Electrochemical and Solid-State Letters*, vol. 9, pp. A228-A231, Mar. 2006.

Spatial-phase-locked Electron-beam Lithography

E. Moon, H.I. Smith, J.T. Hastings (U. Kentucky)
Sponsorship: NSF

Our research in spatial-phase-locked electron-beam lithography (SPLEBL) is conducted in collaboration with the University of Kentucky. It is aimed at reducing pattern-placement errors in electron-beam-lithography systems to the sub-1 nm level. Such high precision is essential for certain applications in photonics and nanoscale science and engineering. The SPLEBL is currently the only approach capable of achieving such pattern-placement accuracy. As shown in Figure 1, SPLEBL uses a periodic signal, derived from the interaction of the scanning e-beam with a fiducial grid placed directly on the substrate, to continuously track the position of the beam while patterns are being written. The SPLEBL senses any deviation of the beam from its intended location on the substrate and feeds corrections to the beam-control electronics to cancel beam-position errors. In this manner, the locations of patterns are directly registered to the fiducial grid on the substrate.

The research effort at MIT is now focused on developing the materials and processes for producing the fiducial grid, with the objectives of maximizing the signal-to-noise of the secondary-electron signal derived from the grid; minimizing electron scattering from the grid, which would be deleterious to precision lithography; maximizing the area and absolute accuracy of the grid; and minimizing the cost and inconvenience of producing the grid on substrates of interest. We have determined that signal levels are maximized when the grid is formed from nanoparticles. Substrates have been patterned with in-situ Faraday cups to make accurate measurements of signal to noise for a wide variety of nanoparticle types. To minimize electron scattering, the nanoparticles must be composed of low-atomic-number materials. Fullerenes may be the optimal nanoparticle, but achieving uniform thickness of layers and attaching the fullerenes along the grid lines represents a challenge of attachment chemistry. Scanning-beam interference lithography will be used to produce master grids. A special form of imprint lithography that maintains long-range spatial-phase coherence will be used to transfer attachment-chemistry grid patterns onto substrates of interest. The research effort at the University of Kentucky is focused on processing of the signal from the grid. Specifically, new approaches are being developed that enable spatial-phase locking while writing in a vector-scan mode. Previous approaches utilized only the raster-scan mode.

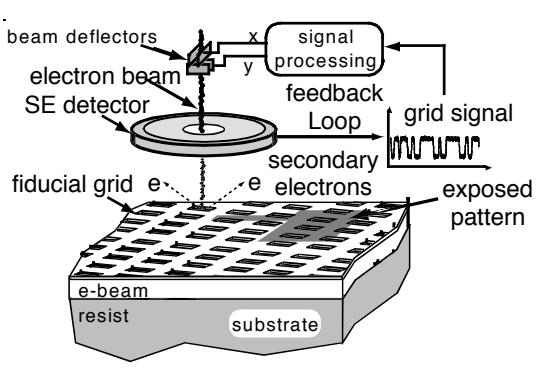

▲ Figure 1: Schematic of the global-fiducial-grid mode of spatial-phase-locked electron-beam lithography. The periodic signal detected from the fiducial grid, which includes both X and Y components, is used to measure placement error, and a correction signal is fed back to the beam deflection system.

REFERENCES

[1] J.T. Hastings, F. Zhang, and H.I. Smith, "Nanometer-level stitching in raster-scanning E-beam lithography using spatial-phase locking," *Journal of Vacuum Science Technology B*, vol. 21, no. 6, pp. 2650-2656, Nov/Dec 2003.

[2] F. Zhang, H.I. Smith, and J.F. Dai, "Fabrication of high-secondary-electron-yield grids for spatial-phase-locked electron-beam lithography," *Journal of Vacuum Science Technology B*, vol. 23, no. 6, pp. 3061-3064, Nov/Dec 2005.

Zone-plate-array Lithography (ZPAL)

R. Menon, S.-Y. Tsai, H.I. Smith
Sponsorship: DARPA, NSF

Optical projection lithography (OPL) has been the key enabler of the continued improvements in performance of silicon integrated electronics. Modern OPL systems are designed for both high resolution and high-volume production, resulting in capital costs of tens of millions of dollars for OPL systems and putting them out of reach for applications other than high-volume production. Moreover, to achieve high resolution, various resolution-enhancement and proximity-effect-correction techniques must be employed. These, in turn, make the cost of masks prohibitive for low-volume production and for research. To address this dilemma, the NanoStructures Lab has for several years been developing an entirely new approach to OPL, depicted in Figure 1, called zone-plate-array lithography (ZPAL)[1]. No mask is required and writing is done in a dot-matrix fashion, which makes proximity-effect correction orders-of-magnitude simpler computationally.

In ZPAL the array of beamlets is created by an array of high-numerical aperture zone plates. The illumination of each zone plate is controlled by one pixel on an upstream spatial-light modulator. This technology is currently being commercialized by LumArray Inc. [2]. Figure 2 shows the roadmap for continued improvement in resolution.

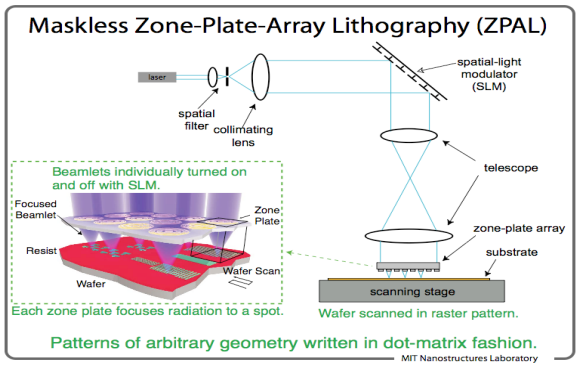

▲ Figure 1: Schematic of zone-plate-array lithography (ZPAL). Light from a CW laser illuminates a spatial-light modulator (SLM), which redirects the light to an array of phase zone plates. These zone plates, in turn, focus the light to diffraction-limited spots on axis, with 40% efficiency. Each pixel of the SLM addresses one zone plate of the array and adjusts the intensity from zero to the maximum in a quasi-continuous manner. By moving the stage and adjusting the intensity of each focal spot under computer control patterns of arbitrary geometry are created in a dot-matrix fashion.

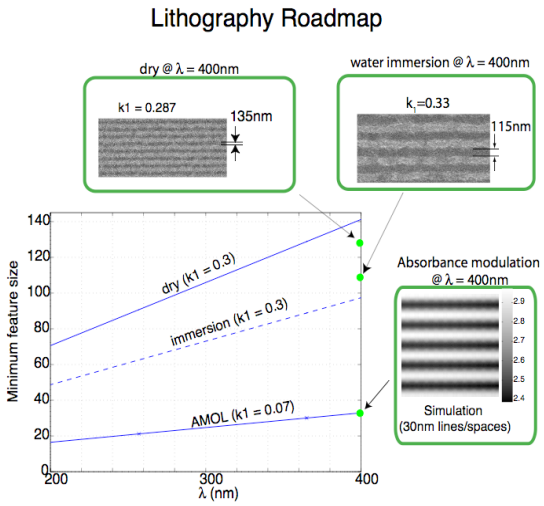

▲ Figure 2: Roadmap for extending ZPAL to the 22 nm node. The micrographs show experimental results for λ = 400 nm. The side plot is a simulation of result expected with Absorbance Modulation Optical Lithography (AMOL) using existing photochromic materials. AMOL is a recent invention at MIT[3][4].

REFERENCES

[1] H.I. Smith, R. Menon, A. Patel, D. Chao, M. Walsh, and G. Barbastathis, "Zone-plate-array lithography: a low-cost complement or competitor to scanning-electron-beam lithography," *Microelectronic Engineering*, vol. 83, pp. 956-961, Apr.-Sep. 2006.

[2] LumArray. [Online]Available : www.lumarray.com.

[3] R. Menon and H.I. Smith, "Absorbance-modulation optical lithography," *Journal of the Optical Society of America A*, vol. 23, pp. 2290-2294, Sep. 2006.

[4] R. Menon, H.-Y. Tsai, and S. W. Thomas III, "Far-field generation of localized light fields using absorbance modulation," *Physical Review Letters*, vol. 98, pp. 043905:1-4, Jan. 2007.

Interference Lithography

T.B. O'Reilly, H.I. Smith
Sponsorship: Internal Funds

Interference lithography (IL) uses the interference of 2 or more coherent light beams to produce periodic structures, such as gratings and grids. Typically, light from a laser is divided and recombined, forming a periodic intensity pattern that can be recorded in a photosensitive film (resist) on a substrate. The NanoStructures Lab (NSL) has been developing interference lithography systems since the mid 1970's, and it operates a range of tools for fabrication gratings, grids, and other periodic structures with periods as fine as 100 nm. These structures have a wide range of applications in nanoscale science and engineering. The most flexible and widely used of our IL systems is the Lloyd's mirror (LM). It can be easily configured to write patterns with periods from 170 nm to several microns. The LM system has recently been used to develop a simple and effective means of testing the response of photoresist to variations in image contrast and exposure dose. Other projects have used patterns from the LM to cut carbon nanotubes, guide the assembly of nanoparticles for templated self-assembly, study the behavior of strained-silicon, or fabricate templates for imprint lithography.

The NSL also operates a Mach-Zehnder interferometer. Although this system lacks the flexibility and ease of use of the Lloyd's mirror, it produces higher quality patterns. The Mach-Zehnder system has been used to study in-plane distortion of silicon nitride membranes and to create super-prisms and super-collimators based on 2D photonic crystals. The NSL also operates an achromatic interference lithography (AIL) system. The AIL uses phase gratings to split and recombine the light from a pulsed, 193-nm ArF excimer laser. It produces 100-nm-period patterns, as shown in Figure 1. This system can form high-contrast fringe patterns over a large area, despite the limited temporal coherence of the ArF laser. The AIL system has been used to create free-standing gratings used in atom-beam interference experiments and EUV spectroscopy.

In addition, the NSL collaborates with the Space Nanotechnology Laboratory, which also operates a Mach-Zehnder IL system and the Nanoruler, an IL system that can write high-quality gratings over areas larger than 300 mm in diameter.

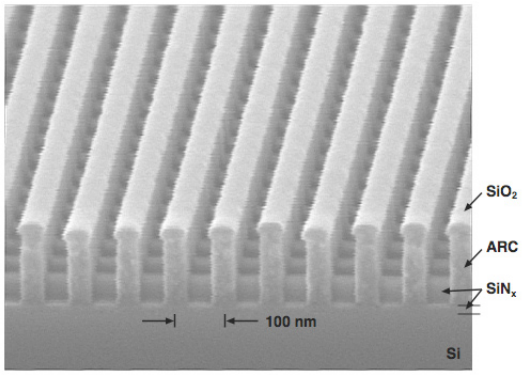

▲ Figure 1: Scanning-electron micrograph of a stage in the fabrication of a 100-nm-period 2D grid, by means of two orthogonal exposures. Note that the underlying grating does not adversely affect the exposure control for the second, orthogonal grating on top.

Immersion-achromatic-interference Lithography

T.B. O'Reilly, M. Walsh, T. Savas, H.I. Smith
Sponsorship: Singapore-MIT Alliance

Interference lithography is a means of using the coherent interference of light to create periodic structures such as gratings and grids. The period of the pattern written is determined by the interference angle, θ, and the wavelength, λ, according to the equation $P = \lambda/2n\sin(\theta)$. Since an upper limit exists for the interference angle (90°), to reduce the period below half the wavelength it is necessary to use an immersion fluid to reduce the effective wavelength of the light. The NanoStructures Lab is developing an immersion-interference-lithography system that will be capable of writing gratings with periods of 70 nm or even smaller.

The system under development, shown in Figure 1, is an achromatic grating interferometer similar to an existing system that is used to produce 100-nm-period gratings. Diffraction gratings are used to split and recombine light in such a way that the contrast of the fringe pattern formed is not dependent on the source's having high spatial or temporal coherence. Analysis of the proposed system has shown that it will be capable of writing gratings with periods as fine as 70 nm, over areas as large as the parent gratings, using water as the immersion fluid. Using immersion fluids of higher index, it should be possible to achieve grating periods as fine as 60 nm (i.e., lines and spaces of 30-nm width). Gratings produced by this system will find application in areas such as atom interferometry, short-wavelength spectroscopy, and templated self-assembly of macromolecules. In addition, the system will be used to study the performance of photoresists and immersion fluids at very high numerical apertures.

To produce a system with reasonable exposure times, the parent gratings must have high diffraction efficiency. Efficiency depends on the dimensions of the grooves that constitute the parent gratings. Diffraction from the gratings has been modeled using the rigorous-coupled-wave analysis method. The resulting designs present a fabrication challenge, requiring the etching of high-aspect-ratio slots in silica glass. New processing techniques have been developed to produce such parent gratings.

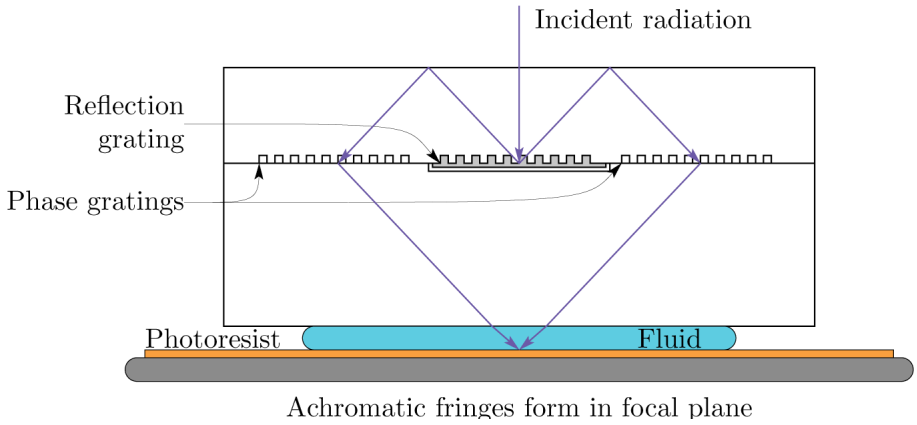

▲ Figure 1: Immersion-achromatic-interference lithography system.

Absorbance-modulation Optical Lithography (AMOL)

R. Menon, H-Y. Tsai, H.I. Smith
Sponsorship: DARPA

We are investigating absorbance modulation as a means to overcome the diffraction limit in far-field, optical-projection imaging. A substrate is coated with an absorbance-modulation layer (AML) in which illumination at one wavelength, λ_2, renders the AML opaque, while illumination at a shorter wavelength, λ_1, renders it transparent. When illuminated with a ring-shaped spot at λ_2 co-incident with a focused spot at λ_1, the dynamic competition between λ_1 and λ_2 results in a nanoscale aperture, through which λ_1 can penetrate to the substrate beneath (see Figure 1). The size of the aperture is limited only by the photokinetic parameters of the AML and the intensities of the illuminations [1].

If the AML is placed atop a photoresist that is sensitive to λ_1 but not to λ_2, patterns of arbitrary geometry can be written by scanning the substrate. The writing speed can be increased by using a large number of independently illuminated lenses operating in parallel and scanning the stage [2]. This technology, which we call Absorbance-Modulation Optical Lithography (AMOL), will be maskless, fast, nanoscale and low-cost. The resolution of AMOL is determined by the ratio of the intensities at the two wavelengths. By simply scaling this ratio, it is possible to scale the transmitted spot far beyond the diffraction limit, enabling AMOL to eventually replace scanning-electron-beam lithography.

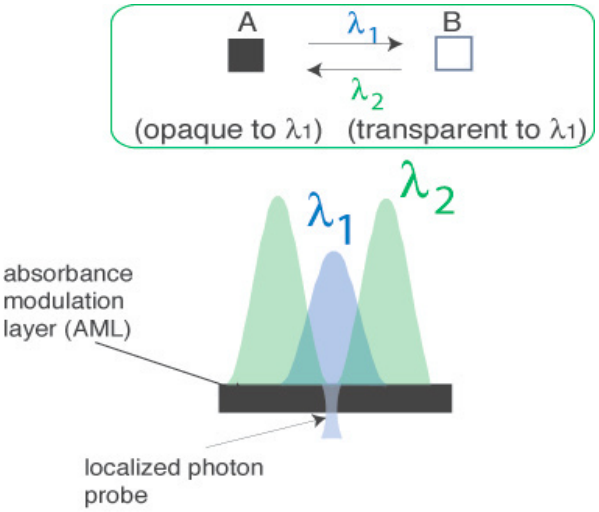

▲ Figure 1: Absorbance modulation. The absorbance modulation layer can be made transparent or opaque, depending upon the wavelength of illumination. By illuminating with both wavelengths at appropriate intensities, a stable, transparent aperture of nanoscale dimensions can be generated as shown.

REFERENCES

[1] R. Menon and H. I. Smith, "Absorbance modulation optical lithography," *Journal of the Optical Society of America A*, vol. 23, p. 2290, Sep. 2006.

[2] R. Menon, H-Y Tsai, and S. W. Thomas III, "Far-field generation of localized light fields using absorbance modulation," *Physical Review Letters*, vol. 98, pp. 043905:1-4, Jan. 2007.

[3] H. I. Smith, R. Menon, A. Patel, D. Chao, M. Walsh, and G. Barbastathis, "Zone-plate-array lithography: a low-cost complement or competitor to scanning-electron-beam lithography," *Microelectron. Eng.*, vol. 83, p. 956, Apr.-Sep. 2006.

Fabrication of 100-nm Pitch Inverted Pyramid Arrays for Templated Self-assembly

T. Savas, H.I. Smith
Sponsorship: Singapore-MIT Alliance

Arrays of inverted pyramids of 100-nm pitch are produced by anisotropically etching silicon through holes in a thin silicon nitride masking layer. The holes in the silicon nitride are patterned with Achromatic Interference Lithography (AIL). The AIL uses diffraction gratings to split and recombine an ArF laser beam of 193-nm wavelength [1]. The recombined beams produce a 100-nm-period grating (lines and spaces), which is recorded in PMMA resist. Grids (posts or holes) can be patterned by recording two orthogonal grating images.

It is well known that an array of holes is most easily obtained by recording the two orthogonal grating images in a negative resist. However, robust, high-resolution negative resists, for lithography at 193 nm, are not available. Therefore, we currently use a positive resist, PMMA, for AIL at 193 nm and pattern holes in the silicon nitride by etching two orthogonal gratings into the nitride.

The inverted pyramids represent artificial structures with facets that are nearly atomically smooth and apices that are close to atomically sharp. They are used in a variety of experiments on templated self-assembly and for producing arrays of crystallographically aligned metallic nanoparticles [2].

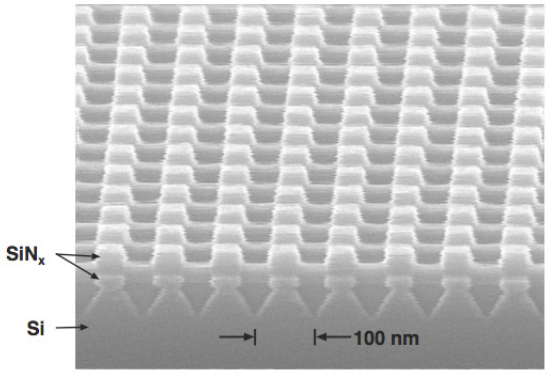

▲ Figure 1: Scanning-electron micrograph showing the pattern in SiN_x on top of (100) Si in which the inverted pyramids have been etched. The SiNx is produced by reactive ion etching following achromatic interference lithography.

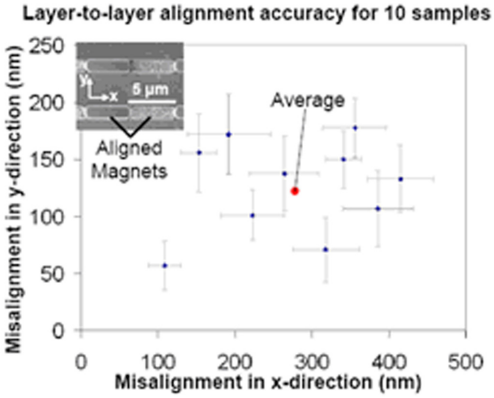

▲ Figure 2: Scanning-electron micrograph of an array of inverted pyramids etched in Si. For templated self-assembly, the Si is lightly oxidized and material to be assembled is deposited on top and annealed.

REFERENCES

[1] T.A. Savas, M.L.Schattenburg, J.M. Carter, and H.I. Smith, "Large-area achromatic interferometric lithography for 100-nm period gratings and grids, with novel applications," *Journal of Vacuum Science Technology B*, vol. 14, pp. 4167-4170, Nov. 1996.

[2] A.L. Giermann and C.V. Thompson, "Solid state dewetting for ordered arrays of crystallographically oriented metal particles," *Applied Physics Letters*, vol. 86, pp. 121903:1-3, Mar. 2005

Building Three-dimensional Nanostructures via Membrane Folding

W.J. Arora, A.J. Nichol, G. Barbastathis, H.I. Smith
Sponsorship: ISN, NSF Graduate Research Fellowships

Nanostructured Origami [1] describes a method of fabricating three-dimensional (3D) nanostructures. Nanometer-scale structures are best fabricated with various two-dimensional (2D) lithography techniques. This project investigates the idea of patterning thin membranes in 2D and then folding them up into a 3D configuration. We have developed methods of both folding and aligning patterned silicon-nitride membranes.

Ion implantation can be used to fold membranes. Membranes are implanted locally with a high dose to create a large stress. By varying the implanted ion energy, the implantation depth can be controlled and hence where the stress is generated. This depth control enables one to fold membranes either up or down. In our experiments, helium ions are used because they do almost no sputtering, do not damage the membrane and can be implanted to depths of 20 to 200 nm with low voltages (2-20 kV). Results are shown in Figure 1.

Magnetic forces can be used to both fold and align nanopatterned membranes [2]. Silicon nitride membranes of 1μm thickness and 100 μm×100 μm area were patterned with arrays of 75 nm thick cobalt nanomagnets. The membrane segments were then patterned and released from the substrate, making them free to rotate about compliant torsional hinges. Before folding, a 0.2 tesla external field magnetized the nanomagnets along their long axis. The field was then rotated 180° to create a magnetic torque to fold the membranes. This procedure resulted in the membranes completely folding over into a coarse layer-to-layer alignment of 2 μm.

After coarse alignment is achieved via folding, the nanomagnet arrays on the folded segments interact resulting in a very precise self-aligning force between arrays. Figure 2 shows the alignment results for folding ten samples. As shown in the plot, the magnet array interaction resulted in alignment error of roughly 200 nm. Therefore, the coarse alignment was reduced by a factor of ten. We modeled the dynamics and found that the alignment accuracy can actually be much better than the lithographic patterning accuracy. Therefore, this method may be useful for 3D nano-systems that need feature placement accuracy better than 20 nm, such as 3D nanophotonics, 3D integrated circuits, and 3D memory.

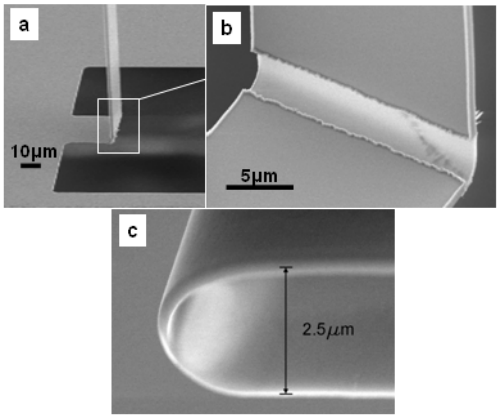

▲ Figure 1: a) A 600-nm SiN_x membrane folded to 90°. b) Magnified view of folded region, which was thinned to 150 nm by CF_4 RIE. The ion implantation was done at 16kV with a dose of 10^{18} ions/cm^2. c) View of a 180° fold illustrating typical fold radius of about 1μm.

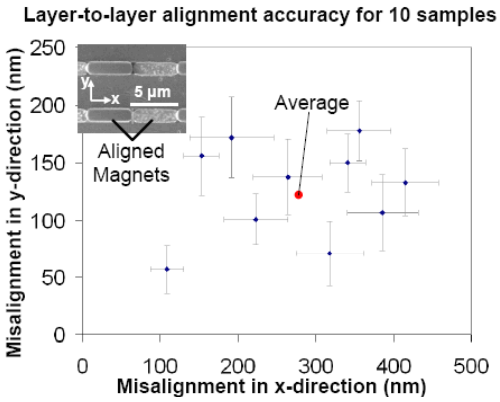

▲ Figure 2: The layer-to-layer alignment error for 100μm ×100μm ×1 μm SiN_x membranes that were folded and aligned using arrays of nanomagnets and an external magnetic field.

REFERENCES

[1] H.J. In, W.J. Arora, T. Buchner, S.M. Jurga, H.I. Smith, and G. Barbastathis, "The nanostructured Origami/sup TM/3D fabrication and assembly process for nanomanufacturing," in *Proc. 4th IEEE Conference on Nanotechnology,* Aug. 2004, pp. 358-60.

[2] A.J. Nichol, P.S. Stellman, W.J. Arora, and G. Barbastathis, "Two-step magnetic self-alignment of folded membranes for 3D nanomanufacturing," *Journal of Microelectronics Engineering,* Dec. 2006, to be published.

Replication of Diffractive-optical Arrays via Imprint Lithography

E.E. Moon, M.D. Galus, R. Menon, H.I. Smith
Sponsorship: Molecular Imprints, Inc.

Diffractive-optical arrays serve important functions in a variety of applications, including zone-plate-array maskless lithography, in which they focus light to diffraction-limited spots and expose multiple features in parallel. Diffractive arrays are typically fabricated by e-beam lithography, but this approach is very time-consuming and prone to defects. We investigated the feasibility of replicating such arrays using a custom step-and-flash imprint lithography (S-FIL) tool [1].

Imprint template patterns were fabricated as relief structures in bulk fused silica, using nickel liftoff after e-beam exposure of PMMA. The nickel pattern was used as a hardmask to dry-etch the patterns into the underlying fused silica. After coating of the template with a release layer, droplets of a low-viscosity imprint fluid were applied to the substrate surface, and the template was leveled and brought to within ~100 nm of the substrate. At that point the imprint fluid filled the template features via capillary action. The imprint fluid was crosslinked under UV exposure, and the template removed. The imprint process was completed in under 5 min. A two-step dry etch transferred the patterns into a transparent substrate. Figure 1 shows micrographs of the resulting imprinted and etched features [2].

The focusing capability of the imprinted diffractive elements was characterized by exposing single-spot features and comparing the feature width, or the derived point-spread function, with a finite-difference time-domain (FDTD) model, as illustrated in Figure 2. We believe these experiments establish the efficacy of imprint lithography for reproduction of diffractive-optical arrays.

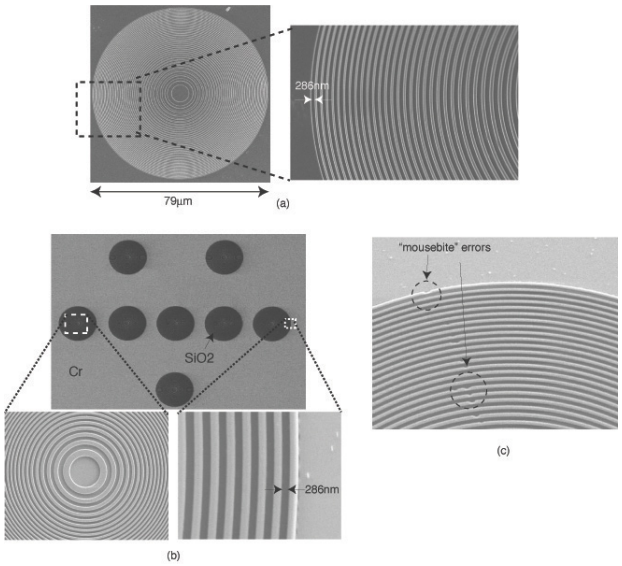

▲ Figure 1: Scanning-electron micrographs of a zone plate imprinted in a fused silica substrate. (a) Imprinted pattern. (b) Etched pattern in fused silica. (c) Close-up view of etched patterns, indicating few local defects ("mousebites"). Moiré artefacts in the micrographs are generated by beating between the scan period of the SEM beam and the spatial periods of the zone plate.

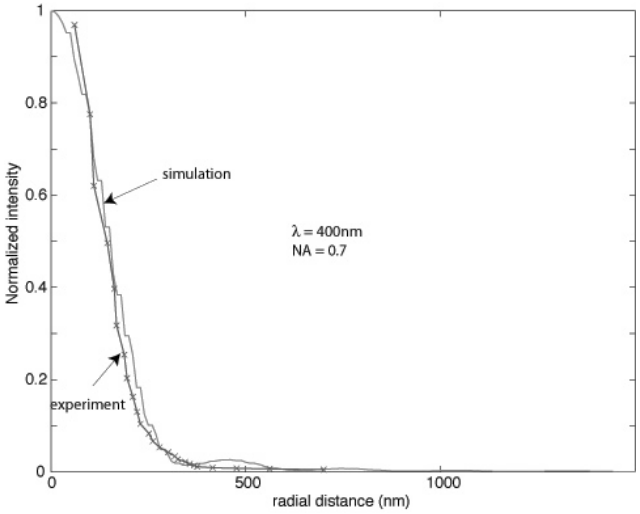

▲ Figure 2: Point-spread function (PSF) characterization of the etched zone plates via single-spot exposures at increasing doses. After scaling, inverse diameters were plotted as a function of the dose. The FDTD-simulated PSF is also plotted for comparison. The parameters were λ = 400 nm, NA = 0.7, f = 40 μm. The data indicate the ability to achieve sub-wavelength focusing using imprinted zone plates.

REFERENCES

[1] E.E. Moon, M.K. Mondol, P.N. Everett, and H.I. Smith, "Dynamic alignment control for fluid-immersion lithographies using interferometric-spatial-phase imaging," *Journal of Vacuum Science Technology B* , vol. 23, p. 2607, Nov. 2005.

[2] M.D. Galus, E.E. Moon, H.I. Smith, and R. Menon, "Replication of diffractive-optical arrays via photocurable nanoimprint lithography," *Journal of Vacuum Science Technology B*, vol. 24, p. 2960, Nov. 2006.

Three-dimensional Photonic Crystals via Membrane Assembly.

A. Patel, H.I. Smith
Sponsorship: NSF

The diffraction of light within periodic structures (so called "photonic crystals") offers a wide variety of opportunities for controlling and manipulating light. Most research to date has focused on 2-dimensional (2D) photonic crystals, because highly developed planar-fabrication techniques (i.e., lithography followed by pattern transfer) are directly applicable. However, the full potential of photonic crystals in futuristic sensing, communication and computation systems is best achieved with 3-dimensional (3D) structures. The problem is that new methods of 3D fabrication need to be developed to achieve desired complex structures over large areas with low cost and high yield.

Interference lithography can produce periodic 3D structures in photosensitive polymers, but the introduction of deviations from perfect periodicity (i.e., waveguides and structures that constitute "devices" within the periodic matrix, so-called "defects") is highly problematic. Moreover, it is not clear that backfilling 3D polymeric structures is applicable to a suitable range of materials. Layer-by-layer methods enable the controlled introduction of defects, but to date fabrication is tedious, slow, low yield, and covers impractically small areas (e.g., <0.1mm on edge).

We describe a novel approach in which the 3D structure is fabricated by assembling membranes that are patterned in advance using conventional planar methods (Figure 1). This approach minimizes the yield problem because membranes can be inspected and selected before assembly, and the desired waveguides and devices can be introduced at any level. When brought into contact, membranes that are free of particulate and other contamination will bond spontaneously by Van der Waals or other mechanisms.

We report the progress to date using low-stress SiN_x membranes as the test vehicle. 2D periodic structures have been etched into-free standing membranes (Figure 2), and nonaligned stacking carried out (Figure 3). We do not consider precise alignment of layers a potential problem since light diffracted from the structures during assembly will provide a built-in, reliable alignment signal. We believe the major problem facing the membrane assembly approach will be ensuring freedom from particles and other contamination. The Si membranes, with their higher refractive index, are more desirable and will be used in the next stage of our research.

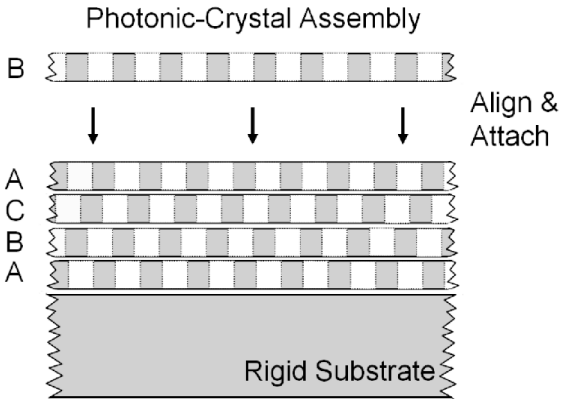

▲ Figure 1: Depiction of the layer-by-layer stacking paradigm we are developing. All the layers in the photonic crystal are fabricated in parallel reducing processing cycles, which will help improve yield and reduce lead times.

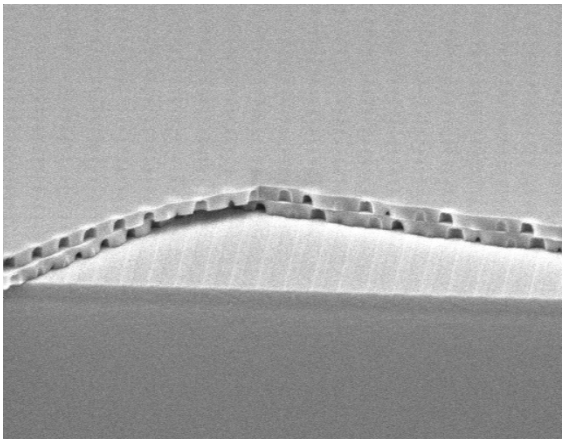

▲ Figure 2: Initial stacking experiment. A patterned SiN membrane is brought into contact with SiN substrate. The pitch of the array is 600 nm and the membrane is 350 nm thick. A second patterned membrane is brought into contact.

Nanofabrication of Hitless Reconfigurable Optical Add-drop Multiplexers in Silicon

T. Barwicz, M.A. Popovic, F. Gan, M. Dahlem, C.W. Holzwarth, P.T. Rakich, E.P. Ippen, F.X. Kaertner, H.I. Smith
Sponsorship: Pirelli S.p.A (Milan, Italy)

Reconfigurable optical add-drop multiplexers (ROADMs) are key components of modern optical networks. Data in optical fibers is carried via numerous wavelengths, referred to as channels. ROADMs allow the rerouting (dropping) of a subset of the data channels traveling in an optical fiber and replacing these with new data streams (adding) that will be carried in the fiber at the previously rerouted wavelengths. The term "reconfigurable" indicates that the subset of dropped channels can be changed in real time while the ROADM is in operation.

Previously, we developed nanofabrication techniques of unprecedented accuracy that allowed us to demonstrate, in silicon-rich silicon nitride, the most advanced micro-ring filters reported to date [1]. In the present work, we employ silicon micro-rings to take advantage of the lower optical loss and high thermo-optical coefficient of silicon. The latter enables wide-range tuning of the wavelengths of operation of the ROADM by means of integrated heaters. Line-edge roughness is of critical concern in silicon waveguides as it translates into optical-propagation loss via scattering of the guided mode. We found that the smoothest waveguides are obtained using hydrogen silsesquioxane (HSQ) as an e-beam resist and etch-mask. Reactive ion etching was done in HBr. Figure 1 is an electron micrograph of the coupling region between a micro-ring and a bus waveguide defined in HSQ. The patterning was done by dose-controlled scanning electron-beam lithography. Figure 2 presents a cross-sectional diagram and top-view micrograph of our implementation of a silicon waveguide with an integrated heater.

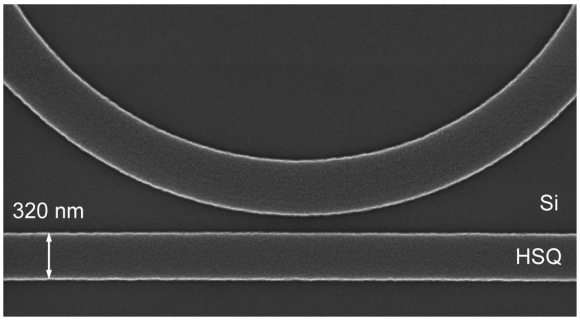

▲ Figure 1: Top-view scanning-electron micrograph of a coupling region defined in HSQ. Line-edge smoothness is critical for Si waveguides. The patterning is based on scanning electron-beam lithography. The minimum feature size required is ~100 nm and must be controlled to ~ 5 nm.

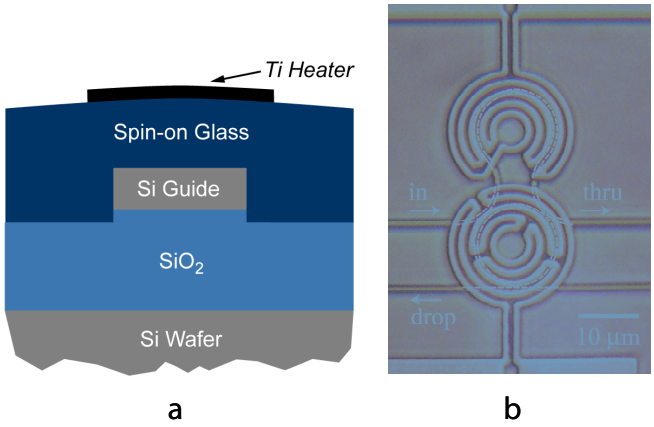

▲ Figure 2: (a) Cross-sectional schematic of a silicon waveguide with an integrated titanium heater. Spin-on glass is used for the upper cladding of the waveguide to allow self-planarization and to avoid filling problems in narrow gaps. (b) Top-view optical micrograph of an overclad silicon-micro-ring filter below a Ti heater.

REFERENCES

[1] M.A. Popovic, T. Barwicz, M.R. Watts, P.T. Rakich, L. Socci, E.P. Ippen, F.X. Kaertner, and H.I. Smith, "Multistage high-order micro-ring-resonator add-drop filters," *Optics Letters*, vol. 31, pp. 2571-2573, Sep. 2006.

Carbene-modified Single-walled Carbon Nanotubes: Electronic Property Control via Chemical Modification

T.M. Wu, B. Long, B. Wunsch, F. Stellacci
Sponsorship: SRC/FCRP IFC

Carbon nanotubes (CNTs) are materials with excellent mechanical, thermal, and electronic properties that may be suitable for electronic devices and interconnects. A potential method for the fabrication of CNT structures on a substrate involves the deposition of CNTs from suspension coupled with chemically-driven alignment or subsequent lithographic processes. As-produced CNTs are notoriously difficult to disperse in solvents, often requiring high-powered sonication or chemical modification that can damage CNT physical and electronic structure. Recently, a covalent chemical functionalization scheme has been proposed [1] that may allow modification of CNTs to impart solubility without the corresponding loss in electronic conductivity observed in other covalent modification schemes. We have fabricated interdigitated electrodes with single-walled carbon nanotubes (SWNTs) to test this theory (see Figure 1), and results indicate that carbene-modified SWNTs are significantly less resistive than SWNTs modified with a standard covalent radical method while remaining more soluble than the as-produced material.

In addition to the conductance-preserving properties of the carbene-CNT chemistry, there is also evidence that the carbene chemistry may shift the Fermi levels of functionalized CNTs. Using an electrochemical open-circuit potential measurement technique, we have observed varying and reproducible steady-state potential values for SWNTs modified with different carbenes (see Figure 2). This approach may allow the development of a chemical doping technique for CNTs where the final Fermi level is determined by the type of substituent on the carbene group.

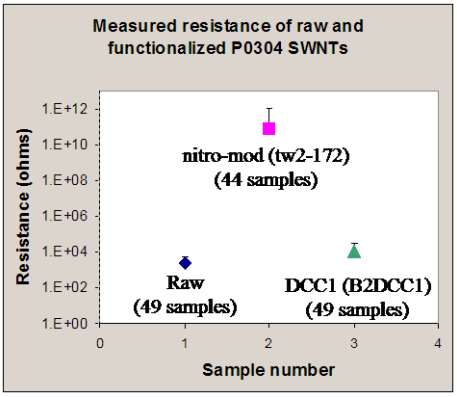

▲ Figure 1: Measured resistance for unmodified and modified SWNTs. The carbene-modified sample (green) show slightly higher resistance than the unmodified sample (blue) but significantly lower resistance than the sample modified with a standard covalent radical method (magenta). Error bars represent two standard deviations.

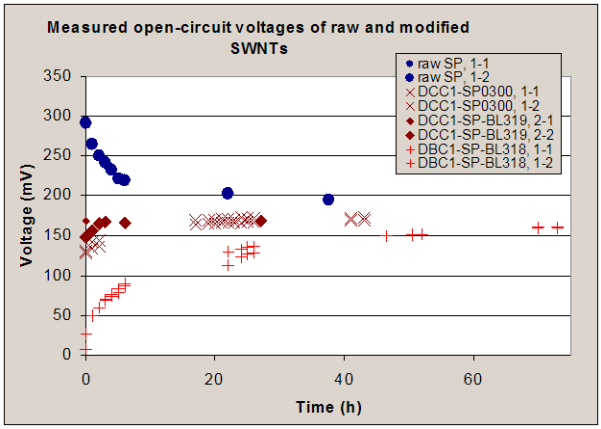

▲ Figure 2: Measured open-circuit potentials for unmodified and modified SWNTs. The unmodified samples are shown in blue. The SWNTs modified with a dichlorocarbene are shown in brown; SWNTs modified with a dibromocarbene are shown in red.

REFERENCES

[1] Y-S. Lee and M. Marzari, "Cycloaddition functionalizations to preserve or control the conductance of carbon nanotubes," *Physical Review Letters*, vol. 97, no. 11, pp. 116801:1-4, Sep. 2006.

Stress Evolution and Defect Formation during Nanoparticle Coalescence

A.R. Takahashi, J. Leib, C.V. Thompson
Sponsorship: NSF, Singapore-MIT Alliance

Metal thin films are key components in a wide variety of micro- and nano-systems. The performance characteristics of thin films are strongly dependent on the intrinsic stress in the film. Figure 1 shows an example of the variation of film stress with film thickness. The tensile stress peak is a key feature in the stress evolution of the film and is associated with the process of particle coalescence [1]. Our computational modeling via molecular dynamics indicates that the magnitude of the stress incorporated during coalescence may be modified by the formation of planar defects [2]. These planar defects relieve strain energy at the expense of stacking fault interface energy. Our calculations also show that planar defects induced by particle coalescence occur only for a specific range of particle sizes. We rationalize the existence of the size window using an analytic energetic model consistent with existing continuum theories for particle coalescence [3]. The presence of stacking faults in coalesced nanoparticles has been confirmed by transmission electron microscopy (TEM); see Figure 2. The planar defects can further reduce the intrinsic stress by changing position within the particle. The TEM observations of partially coalesced structures suggest that the faults anneal out of the particles at high temperatures. Our observations and model show that the intrinsic stress in thin films can be tuned by controlling the particle size at coalescence and defect density.

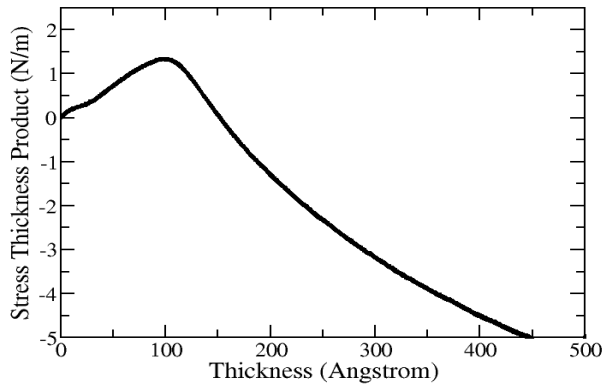

▲ Figure 1: Stress thickness product as a function of Au film thickness on silicon nitride. The tensile peak in the curve is associated with the process of island coalescence.

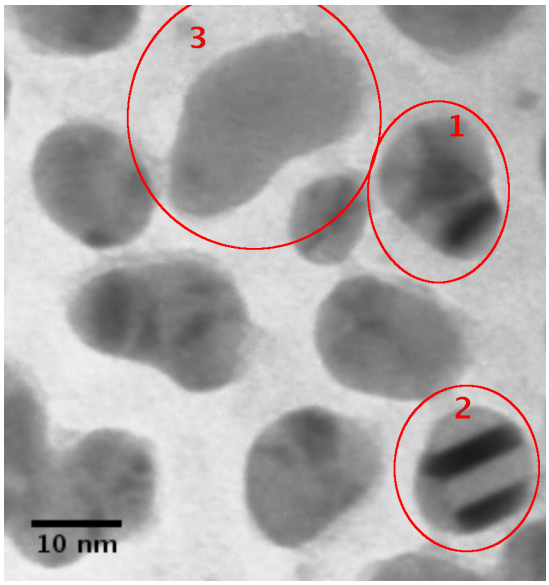

▲ Figure 2: A TEM image of Au nanoparticle structures after 20 Angstroms of deposition. Regions 1 and 2 show particles clearly containing stacking faults. Region 3 shows a larger particle that appears to be defect-free.

REFERENCES

[1] W.D. Nix and B.M. Clemens, "Crystallite coalescence: A mechanism for intrinsic tensile stresses in thin films," *Journal of Materials Research*, vol. 14, no. 8, pp. 3467-3473, Aug. 1999.

[2] A.R. Takahashi, C.V. Thompson, and W.C. Carter, "Metallic island coalescence: Molecular dynamics simulations of boundary formation and tensile strain in polycrystalline thin films," in *Mat. Res. Soc. Symp. Proc.*, San Francisco, CA, Apr. 2003, vol. 779, pp. W4.5.1-W4.5.6.

[3] A.R. Takahashi and C.V. Thompson, "Nanoscale metallic island coalescence and defect formation," to be published.

Templated Dewetting of Nanoparticle Solutions

S.-W. Chang, C.V. Thompson
Sponsorship: Singapore-MIT Alliance

A major issue in nanotechnology is the need for versatile techniques for self-organization of nanometer-scale building blocks, such as nanoparticles, to form large-area periodic systems. Our goal is to combine physical templating and self-assembly to form nanoparticle arrays that can be used as catalysts for the growth of nanowire or nanotube arrays and other applications such as nanoelectronics or nanophotonics.

A combination of physical templating and capillary interaction has been employed to self-organize colloidal particles into lithographically patterned templates with well-controlled sizes and structures. The patterned features can act as pinning sites for the moving contact line, leading to high particle concentrations near the pinning sites. Particles in the physical templates then self-assemble into close-packed structures due to long-range immersion forces.

As an initial effort, patterned substrates with gratings and holes were fabricated using interference lithography. The substrates were then immersed in Au nanoparticle solutions for evaporation. The resulting capillary interaction due to solvent evaporation was found to be sufficiently strong to force the nanoparticles into the templated features without leaving particles on the surrounding areas. Figure 1 presents a schematic outline of the process. Current efforts include applying the templated dewetting approach to smaller nanostructures and on different topographies.

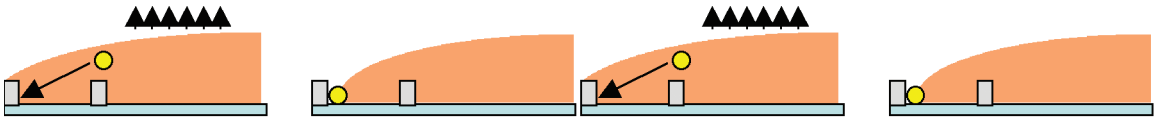

▲ Figure 1: Schematic of the templating process.

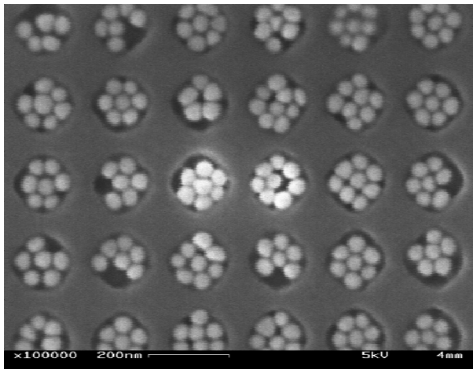

▲ Figure 2: Au particles that are 50 nm in diameter self-assemble into templated holes.

Templated Self-assembly for Nanoparticle Organization: Solid-state Dewetting

A.L. Giermann, J. Ye, Y. Wang, W.K. Choi, H.I. Smith, C.V. Thompson
Sponsorship: Singapore-MIT Alliance, NSF

We are investigating solid-state dewetting of thin films as a technique for producing ordered arrays of metal nanodots over large areas. Such arrays are used as catalysts for nanowire and nanotube growth and may also be of interest in memory or plasmon device applications. Our research comprises two main dewetting systems: 1) polycrystalline films on amorphous substrates and 2) epitaxial films on single crystal substrates.

In our study of polycrystalline films, we influence dewetting behavior with topographically patterned oxidized silicon substrates that modulate the curvature of as-deposited films. Gold films deposited and annealed on di-periodic arrays of pyramidal pits result in one-to-one self-assembly of ordered arrays of gold particles over large areas. Average particles sizes of less than 50 nm can be achieved. Compared to dewetting on flat substrates, the templates impose a significant decrease in average particle size and ensure a narrow size and spatial distribution (Figure 1). This technique uniquely results in crystallographic ordering of the particles, imposing an in-plane texture and changing the out-of-plane texture (Figure 2).

Our current efforts include investigation of other topographic geometries and development of numeric models to predict topographies that lead to the formation of multiple particles per lithographic feature. We are also expanding the technique to nickel, which is known to catalyze carbon nanotube growth, with the goal of studying the impact of crystallographic texture and facet morphology on nanotube growth.

In our study of epitaxial films, we grow nickel thin films on single crystal magnesium oxide substrates and observe the dependence of the dewetting behavior on various experimental parameters, such as crystallographic orientation of the substrate, film thickness, annealing time, and annealing temperature. The crystallographic orientation of the substrate has a profound effect on the evolution and final form of the dewetted film. We believe these differences are associated with surface energy anisotropy of nickel. Dewetting of single crystal films also offers the potential for obtaining ordered arrays of crystallographically aligned catalyst particles.

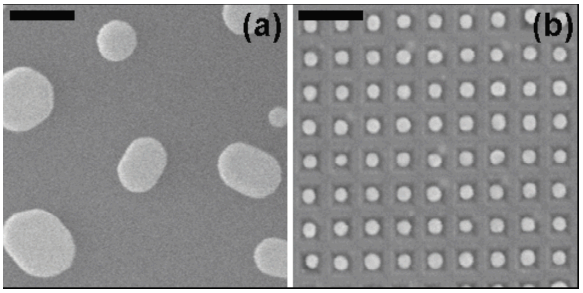

▲ Figure 1: The effect of topography on particle morphology. The results of dewetting a 10-nm-thick Au film on (a) a flat substrate and (b) a topographic substrate. Micrographs are displayed at the same magnification to emphasize the effect of topography on particle size. Scale bars are 200 nm in length.

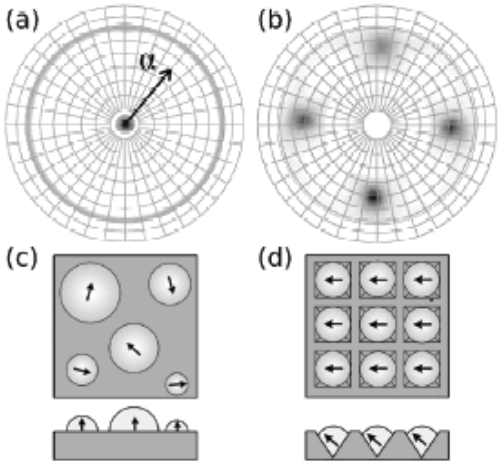

▲ Figure 2: The effect of topography on particle orientation. (a) and (b) show Au <111> X-ray pole figures (37.4° < 2θ < 38.6°), (a) for particles on a flat substrate and (b) for particles on a topographic substrate. (c) and (d) schematically illustrate the particle orientation on flat and topographic substrates, respectively. The arrows indicate the <111> projection.

REFERENCES

[1] A.L. Giermann and C.V. Thompson, "Solid-state dewetting for ordered arrays of crystallographically oriented metal particles," *Applied Physics Letters*, vol. 86, no. 12, pp. 121903:1-3, Mar. 2005.

Anodic Aluminum Oxide Scaffolds for Realization of Integrated Self-assembled Devices

J. Oh, C.V. Thompson
Sponsorship: SRC/FCRP IFC, Singapore-MIT Alliance

Nano-sized materials are core building blocks for advanced functional devices such as interconnects, logics, memories, sensors, and displays. To integrate synthesized nano-materials into the devices, it is desirable to fabricate them with controlled size and distribution on the device applicable substrates with precise location. As a strategy, we are developing templated self-assembly methods that combine top-down (lithography) and bottom-up (self-assembly) approaches for fabricating and assembling metallic and semiconducting nano-wires, rods, and dots, for new applications including nano-contacts for devices and interconnects for mixed-material and multifunctional micro- and nano-systems.

Anodic aluminum oxide (AAO) is a self-ordered nanostructured material that is well-suited as a scaffold to grow multi-functional nanowires and nanotubes for use in magnetic, electronic and opto-electronic devices. Perfectly ordered porous alumina scaffolds were developed by combining interference lithography with anodization of the evaporated Al thin films on silicon substrates. The regular array of electrically insulating holes obtained had diameters of less than 30 nm and aspect ratios >50:1, which is hardly achievable without the state-of-art Si technology. Topographic templating of long-range order in anodic aluminum oxide allows independent control of the pore size, spacing, and order symmetry in ranges not achievable without templating. Using the perfectly-ordered AAO scaffolds, we have fabricated ordered metallic nanodots, nanorods, and nanotubes as well as well-aligned multi-walled carbon nanotubes (CNTs) on silicon substrates. In addition to the vertically ordered AAO scaffolds, we are also developing the porous alumina scaffold, horizontally lying on the substrate to grow nano-materials on the plane of substrate.

We are currently pursuing the growth of uniform arrays of CNTs in templated AAO scaffolds to obtain statistical electrical and thermal characterization of CNTs as a function of nanotube diameter and length variations

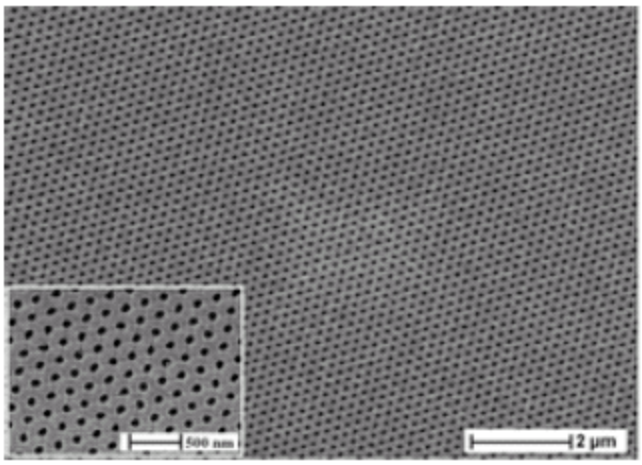

▲ Figure 1: An SEM image of perfectly ordered porous alumina with hexagonal symmetry on silicon over wafer-scale areas with pore diameter of 80 nm and pore spacing of 180 nm [1]

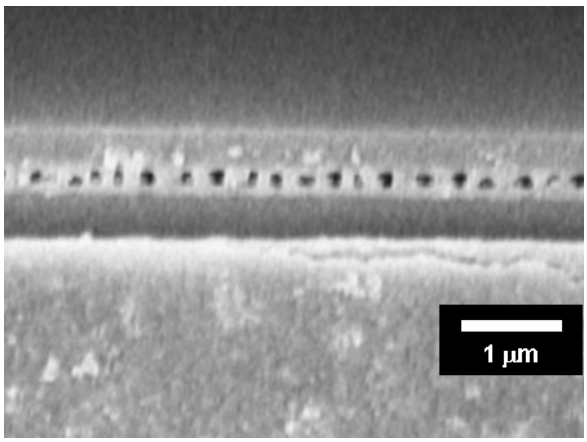

▲ Figure 2. An SEM image of a monolayer of porous alumina lying horizontally on the substrate.

REFERENCES

[1] R. Krishnan, H.Q. Nguyen, C.V. Thompson, W.K. Choi, and Y. L. Foo, "Wafer-level ordered arrays of aligned carbon nanotubes with controlled size and spacing on silicon," *Nanotechnology*, vol. 16, pp. 841-845, June 2005.

Catalyst Engineering and Carbon Nanotube Growth Mechanisms

G.D. Nessim, Y. Wang, A.J. Hart, D. Acquaviva, J. Oh, J.S. Kim, C. Morgan, N. Abate, M. Seita, C.V. Thompson
Sponsorship: SRC/FCRP IFC, Intel Corporation

As integrated circuit technology is developed at dimensions below 45 nm, carbon nanotubes (CNTs) represent an ideal replacement for copper interconnects as they can carry higher current densities, do not need liners, and do not suffer from electromigration. However, fabrication issues such as growing the desired type of CNTs in a selected position and making electrical contacts and interconnections remain major technical challenges.

Consistent with our goal of making the use of carbon nanotubes a manufacturing reality for interconnect vias, we have achieved the following results:

We discovered that by introducing the reducing gas (hydrogen) at specific times during the thermal chemical vapor deposition process, we were able to control the diameter and the number of walls of vertically-aligned CNTs grown on insulating substrates, as shown by Transmission Electron Microscopy images. We also analyzed the substrate with Atomic Force Microscopy to correlate catalyst morphology with CNT density.

Using appropriate catalyst/substrate metallic thin films, we have grown carbon nanostructures at temperatures below 500 degrees Celsius. We analyzed properties such as the grain structure of the substrate to maximize CNT density and achieve vertical alignment. Electrical measurements show contact of the CNTs with the conductive substrate.

Finally, we have grown CNTs on conductive substrates in an insulating anodized alumina scaffold with perfectly periodic templated pores. This technique will allow us to emulate a nanometer-scale via system for measurement of electrical and thermal properties of CNTs, averaged over a large regular matrix. We plan to use this structure to develop CNT-based devices.

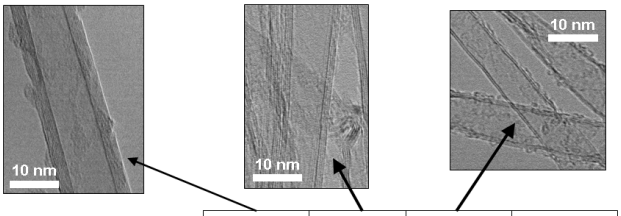

	H_2 @ -5	H_2 @ 0	H_2 @ +10	H_2 @ +13
Outer diameter [nm]	13.6 ±1.9	9.8 ±1.8	7.4 ±1.0	8.1 ±1.3
Number of walls	7.3 ±1.1	4.7 ±1.0	3.0 ±0.9	3.1 ±1.0
CNT areal density [/cm^2]	3.9×10^9	2.6×10^{10}	4.9×10^{10}	4.5×10^{10}
Growth rate [μm/min]	32	37	154	**440**

▲ Figure 1: Transmission electron microscope images of multi-wall carbon nanotubes grown using iron catalysts on alumina substrates using the same process but delaying the introduction of hydrogen. As the delay in hydrogen introduction is increased (up to a limit), the diameters and number of walls of the tubes reduces, and the length and number of tubes per area increases.

Fiber Composites Reinforced by Aligned CNTs

E.J. Garcia, A.J. Hart, B.L. Wardle (in coll. with A.H. Slocum)
Sponsorship: Airbus S.A.S., Karl Chang Innovation Fund, La Caixa Foundation

The interaction, or wetting, of long aligned carbon nanotube (CNT) forests with off-the-shelf (no solvent added) commercial thermoset polymers is investigated experimentally. A technique for creating vertically aligned CNT composite microstructures of various shapes is presented [1]. Direct characterization of the mechanical properties of the nanocomposites structures is also presented in this work. The mechanical reinforcement results (220% increase of the Young´s modulus at 2% volume loading [2]) support the feasibility of using these CNT forests in large-scale, hybrid, advanced composite architectures reinforced with aligned CNTs.

A hybrid composite architecture consisting of aligned carbon nanotubes (CNTs), woven ceramic fiber cloth, and a thermoset epoxy is described and fabricated. Interlaminar reinforcement improvement is also quantified experimentally [3]. The nano-engineered laminates are constructed using conventional hand lay-up techniques. Fabrication begins with growth of aligned CNTs on the surface of fibers in a ceramic fiber cloth using a thermal chemical vapor deposition process and liquid-based catalyst as shown in Figure 1. Effective wetting of the CNT/cloth by the polymer is shown via optical and scanning electron microscopy (see Figure 2). This intralaminar reinforcement by CNTs also extends to the interlaminar region between individual plies in the laminate. The strength of the interlaminar reinforcement is investigated experimentally, focusing on shear strength with an average improvement of 70% over the unreinforced laminate. Ongoing investigations focus on such nano-engineered laminates, including mechanical and multifunctional performance benefits derived from the aligned nature of the CNTs appearing everywhere in the laminate. Future work focuses on extending this model architecture to carbon- fiber-based advanced composites.

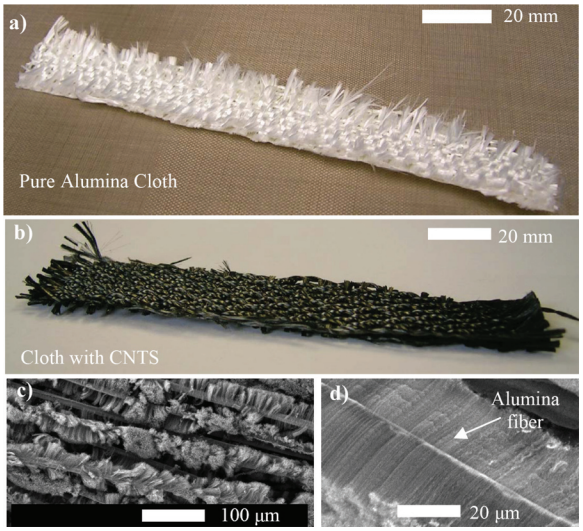

▲ Figure 1: a) As-received alumina cloth; b) Alumina cloth with CNTs grown on the surface of fibers; c) An SEM of the alumina fibers with CNTs grown on the surface; d) An SEM of one alumina fiber with well-aligned, 30-µm long CNTs grown on its surface.

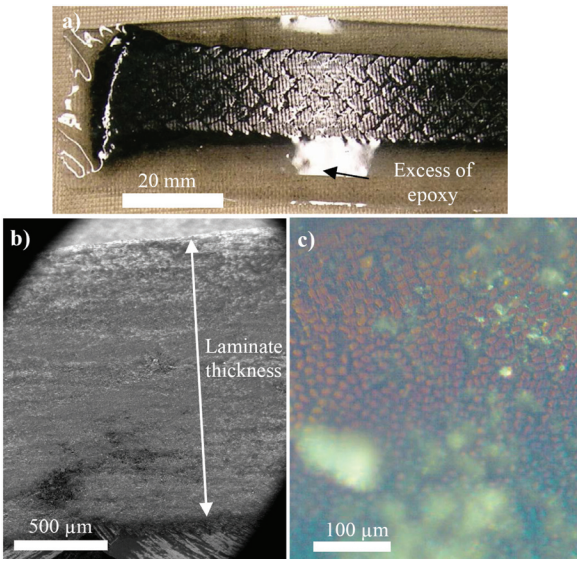

▲ Figure 2: a) Nanoengineered composite laminate before cutting the specimen for inspection; b) An SEM picture of a cross section of CNT/alumina cloth/epoxy hybrid composite with no evidence of voids; c) Optical microscopy picture of the cross section, showing regular distribution (volume fraction) of the fibers inside the cloth.

REFERENCES

[1] E.J. García, A.J. Hart, B.L. Wardle, A.H. Slocum, "Fabrication of composite microstructures by capillarity-driven wetting of aligned carbon nanotubes with polymers," *Nanotechnology*, vol. 18, no. 16, pp. 165602:1-11, Apr. 2007.

[2] E.J. García, A.J. Hart, B.L. Wardle, A.H. Slocum, "Fabrication and nanocompression testing of aligned CNT/polymer nanocomposites," *Advanced Materials*, 2007, to be published.

[3] E.J. García, A.J. Hart, B.L. Wardle, A.H. Slocum, "Aligned carbon nanotube reinforcement of ply interfaces in woven composites," presented at the *48th AIAA/ASME/ASCE/AHS/ASC Structures, Structural Dynamics, and Materials Conference*, Apr. 2007.